Neuron

Article

Upregulation of *SYNGAP1* expression in mice and human neurons by redirecting alternative splicing

Graphical abstract

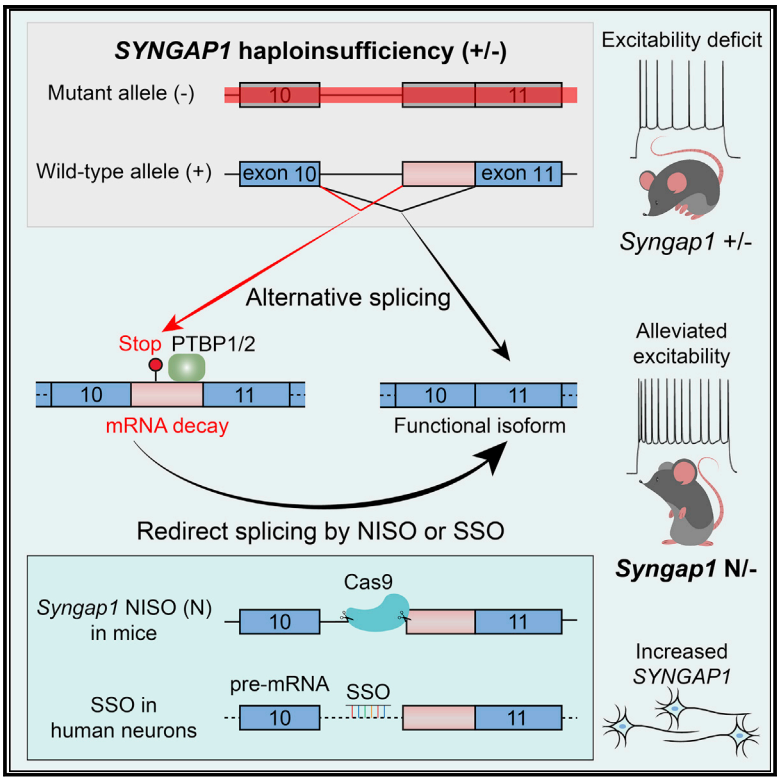

Highlights

- *SYNGAP1* alternative 3′ splice site induces nonsense-mediated mRNA decay (A3SS-NMD)
- PTBP1/2 proteins suppress *SYNGAP1* by promoting A3SS-NMD
- Deleting A3SS-NMD alleviates deficits in heterozygous *Syngap1* knockout mice
- Splice-switching oligonucleotide targeting the A3SS upregulates *SYNGAP1* expression

Authors

Runwei Yang, Xinran Feng, Alejandra Arias-Cavieres, ..., Christian Hansel, Alfredo J. Garcia III, Xiaochang Zhang

Correspondence

xczhang@uchicago.edu

In brief

De novo SYNGAP1 **mutations cause autism, epilepsy, and intellectual disability. Yang et al. show that PTBP1/2 proteins promote *SYNGAP1* mRNA decay through alternative splicing. Redirecting splicing upregulates *Syngap1* expression and alleviates neurological deficits in *Syngap1* heterozygous knockout mice, suggesting that redirecting splicing can potentially rescue *SYNGAP1* haploinsufficiency.**

Yang et al., 2023, Neuron *111*, 1–14
May 17, 2023 © 2023 Elsevier Inc.
https://doi.org/10.1016/j.neuron.2023.02.021

CellPress

Please cite this article in press as: Yang et al., Upregulation of *SYNGAP1* expression in mice and human neurons by redirecting alternative splicing, Neuron (2023), https://doi.org/10.1016/j.neuron.2023.02.021

Neuron

CellPress

Article

Upregulation of *SYNGAP1* expression in mice and human neurons by redirecting alternative splicing

Runwei Yang,[1,6] Xinran Feng,[1,6] Alejandra Arias-Cavieres,[2] Robin M. Mitchell,[3] Ashleigh Polo,[2] Kaining Hu,[1] Rong Zhong,[1] Cai Qi,[1] Rachel S. Zhang,[1] Nathaniel Westneat,[1] Cristabel A. Portillo,[3,4] Marcelo A. Nobrega,[5] Christian Hansel,[3] Alfredo J. Garcia III,[2] and Xiaochang Zhang[1,7,*]

[1]Department of Human Genetics, Neuroscience Institute, The University of Chicago, Chicago, IL 60637, USA
[2]Section of Emergency Medicine, Department of Medicine, Institute for Integrative Physiology, Neuroscience Institute, The University of Chicago, Chicago, IL 60637, USA
[3]Department of Neurobiology, Neuroscience Institute, The University of Chicago, Chicago, IL 60637, USA
[4]Department of Anatomy and Neurobiology, University of California Irvine, Irvine, CA 92697, USA
[5]Department of Human Genetics, the University of Chicago, Chicago, IL 60637, USA
[6]These authors contributed equally
[7]Lead contact
*Correspondence: xczhang@uchicago.edu
https://doi.org/10.1016/j.neuron.2023.02.021

SUMMARY

The Ras GTPase-activating protein *SYNGAP1* plays a central role in synaptic plasticity, and *de novo SYNGAP1* mutations are among the most frequent causes of autism and intellectual disability. How *SYNGAP1* is regulated during development and how to treat *SYNGAP1*-associated haploinsufficiency remain challenging questions. Here, we characterize an alternative 3′ splice site (A3SS) of *SYNGAP1* that induces nonsense-mediated mRNA decay (A3SS-NMD) in mouse and human neural development. We demonstrate that PTBP1/2 directly bind to and promote *SYNGAP1* A3SS inclusion. Genetic deletion of the *Syngap1* A3SS in mice upregulates Syngap1 protein and alleviates the long-term potentiation and membrane excitability deficits caused by a *Syngap1* knockout allele. We further report a splice-switching oligonucleotide (SSO) that converts *SYNGAP1* unproductive isoform to the functional form in human iPSC-derived neurons. This study describes the regulation and function of *SYNGAP1* A3SS-NMD, the genetic rescue of heterozygous *Syngap1* knockout mice, and the development of an SSO to potentially alleviate *SYNGAP1*-associated haploinsufficiency.

INTRODUCTION

Synaptic transmission and plasticity are fundamental to neuronal functions, and alterations of synaptic protein expression are direct causes of autism, intellectual disability (ID), and epilepsy.[1,2] *De novo* loss-of-function (LoF) mutations in *SYNGAP1*, encoding the synaptic Ras GTPase-activating protein,[3,4] are among the most prevalent causes of ID and autism spectrum disorders.[5–7] Previous human and mouse studies on *SYNGAP1* pathogenic mechanisms converge on that *de novo* mutations are predominantly LoF alleles and lead to *SYNGAP1* haploinsufficiency.[7–9] The development of treatment for *SYNGAP1*-associated conditions has a far-reaching impact.

Syngap1 was initially identified by sequencing proteins in the postsynaptic density (PSD) or interacting with PDZ domains.[3,4] Syngap1 suppresses ERK phosphorylation and surface AMPA receptor levels[10,11]; phosphorylation of Syngap1 by CaM Kinase II rapidly disperses Syngap1 from synaptic spines and triggers AMPA receptor insertion.[3,12] Homozygous *Syngap1* knockout (*Syngap1* −/−) mice died within 48 h after birth; heterozygous *Syngap1* knockout led to ∼50% reduction of Syngap1 protein, reduced long-term potentiation (LTP), impaired membrane excitability, decreased ability in spatial learning, and reduced cognition primarily due to defects in forebrain excitatory neurons.[13–16] Loss of Syngap1 in GABAergic cells was also reported to impair cognitive functions.[17] Mechanistically, *Syngap1* heterozygous knockout mice exhibited increased excitatory synaptic transmission in early postnatal development due to enhanced AMPA receptor sensitivity.[9] The re-expression of Syngap1 in adult mice slightly improved brain functions and behaviors,[18] implying that upregulating SYNGAP1 protein expression in the brain can potentially alleviate symptoms in human patients with *SYNGAP1* haploinsufficiency.

Alternative splicing coupled with nonsense-mediated mRNA decay (AS-NMD), or unproductive splicing, is frequently used by RNA splicing regulators as a negative autofeedback for

Please cite this article in press as: Yang et al., Upregulation of *SYNGAP1* expression in mice and human neurons by redirecting alternative splicing, Neuron (2023), https://doi.org/10.1016/j.neuron.2023.02.021

homeostatic protein expression.[19,20] AS-NMD is predicted to regulate hundreds of genes in mammalian brains,[21] but its role in human and mouse brain development has only started to be explored recently.[22–24] In past years, splice-switching oligonucleotides (SSOs) targeting genes such as *SMN2* have been successful in treating neurological disorders,[25,26] paving the path for SSO-mediated therapy and personalized medicine.[27] In our efforts to study cell-type-specific alternative splicing, we identified an alternative 3′ splice site (A3SS) of *SYNGAP1* intron 10 that led to NMD in mouse and human brain development, hereafter referred to as *Syngap1* A3SS-NMD. Alternative splicing was suggested as a potential way to modulate SYNGAP1 protein expression in HEK293 cells,[28] but it remains unclear to what extent SSO works in human neurons. More importantly, as a safety measure, it is essential to understand the organismal function and dosage effect of *Syngap1* A3SS-NMD *in vivo* before targeting this exon for therapy.

We have characterized *Syngap1* A3SS-NMD inclusion in brain development and investigated regulatory mechanisms. We identified intronic sequences required for *Syngap1* A3SS-NMD inclusion, and genetic deletion of such sequences in mice resulted in the skipping of A3SS-NMD and enrichment of the neuronal isoform; therefore, we named this mouse allele *Syngap1-NISO* (Neuronal ISOform). Notably, we detected decreased A3SS-NMD inclusion and increased Syngap1 protein expression in *Syngap1-NISO* mouse brains and SSO-treated cerebral organoids. In this study, we investigate the functions of *Syngap1* A3SS-NMD *in vivo* and explore whether the A3SS-NMD exon is a possible target to rescue haploinsufficiency.

RESULTS

Alternative splicing of mouse *Syngap1* intron10 leads to nonsense-mediated mRNA decay

We investigated cell-type-specific alternative splicing during neocortical development at embryonic day 14.5 (E14.5) and identified an A3SS of *Syngap1* intron10 (Figure 1A). We examined the *Syngap1* A3SS in mouse development and found that the inclusion level was high in non-neural tissues and during early brain development but decreased substantially in the adult brain (Figure 1B). RT-PCR of the *Syngap1* A3SS showed 76% inclusion at E12.5 and 5% inclusion at postnatal day 40 (P40, Figure 1C). Notably, intronic sequences around the *Syngap1* A3SS are conserved in vertebrates, suggesting a selection pressure during evolution (Figure 1B, bottom track). In cultured primary cortical neurons, the *Syngap1* A3SS showed 33% ± 5% usage at day 1 *in vitro* (DIV1) and decreased to 5% ± 1% at DIV15 (Figure S1A). These results suggest that the *Syngap1* A3SS is included in mouse brain development and remains detectable in differentiated neurons.

Surprisingly, the *Syngap1* A3SS introduces in-frame translational stop codons, which are predicted to truncate the RasGAP domain or cause NMD (Figure 1D). Multiple lines of our results support that *Syngap1* A3SS causes NMD (A3SS-NMD): (1) the predicted premature stop codons are over 50 base pairs away from downstream splice junctions (Figure 1D), (2) an antibody against the N terminus of Syngap1 recognized the ectopically expressed Syngap1 N-terminal fragment and the endogenous full-length protein but was unable to detect the truncated isoform from brain lysates (Figure 1E), (3) the *Syngap1* A3SS isoform was enriched when NMD was blocked by inhibiting protein translation with cycloheximide (CHX) in Neuro2a cells and in primary neurons (Figures 1F and S1B), and (4) *Syngap1* A3SS was upregulated when NMD was blocked by knocking down *Upf1* with two different siRNAs in Neuro2a cells (Figures 1G and S1C). These results indicate that *Syngap1* A3SS causes NMD, whereas the canonical neuronal splice isoform ensures robust protein expression.

SYNGAP1 unproductive splicing is functionally conserved in humans

To determine whether human *SYNGAP1* is regulated by A3SS in cortical development, we compared RNA-seq data between the ventricular zone (VZ, enriched for neural progenitors) and cortical plate (CP, enriched for post-mitotic neurons) of the gestational week 16 (GW16) fetal human brains.[29] The *SYNGAP1* A3SS showed higher inclusion in the VZ than in the CP (Figure 2A). This was further confirmed using RT-PCR with microdissected VZ and CP samples from multiple postmortem fetal dorsal forebrains (Figure 2B). We analyzed the human *SYNGAP1* RNA-seq reads and confirmed the inclusion of premature stop codons (Figure S2A). We further examined human *SYNGAP1* A3SS inclusion during induced pluripotent stem cell (iPSC)-to-neuron differentiation and found the *SYNGAP1* A3SS remained 23% ± 2% in NGN1/2-induced neurons at day 4 (Figures 2C and S2B). CHX treatment in iPSCs and iPSC-derived neurons significantly increased *SYNGAP1* A3SS transcripts (Figures 2D and 2E). Although the human *SYGNAP1* transcript was also detectable in non-neural tissues (GTEx), the *SYNGAP1* A3SS-NMD provides an orthogonal mechanism to ensure neural-specific expression of SYNGAP1 protein. Multiple sequence alignment of mammalian *SYNGAP1* intron10 showed that the premature stop codon (TGA) introduced by the A3SS was highly conserved, although the positions of alternative 3′ splice sites varied among different species (Figure 2F). These results indicate that the *SYNGAP1* A3SS-NMD is functionally conserved in human neural development.

Human mutations causing *SYNGAP1* unproductive splicing are associated with ID and autism

To understand whether the *SYNGAP1* A3SS-NMD is functional in humans, we focused on two previously reported *SYNGAP1* mutations in intron10: these mutations were identified in patients with typical ID and autistic features; however, the effects of these mutations on *SYNGAP1* expression were not well understood.[7,30] We constructed wild-type and mutant *SYNGAP1* mini-genes (spanning exon9 to exon12), introduced the constructs into Neuro2a cells, and found that the c.1676+5 G>A (NM_006772.2) mutation almost completely disrupted the splice donor and induced high intron10 retention (Figures 2G and 2H). The pathogenic c.1677-2_1685del mutation disrupted the canonical splice acceptor of intron 10 and significantly increased *SYNGAP1* A3SS usage (Figures 2G and 2H). Thus, human mutations that lead to *SYNGAP1* A3SS-NMD or intron10 retention could result in autism and ID, suggesting that the *SYNGAP1* A3SS-NMD transcript is not functional *in vivo*.

Please cite this article in press as: Yang et al., Upregulation of *SYNGAP1* expression in mice and human neurons by redirecting alternative splicing, Neuron (2023), https://doi.org/10.1016/j.neuron.2023.02.021

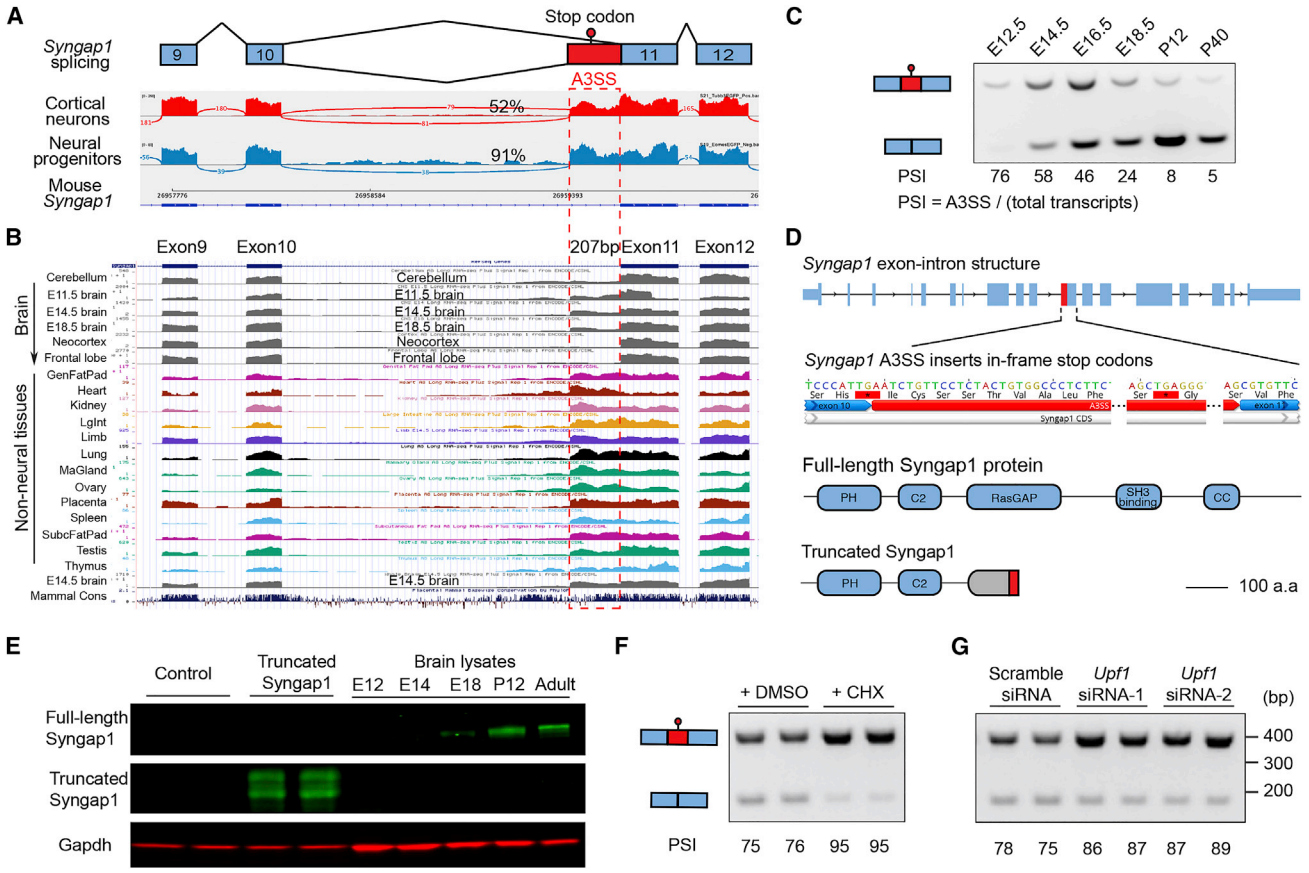

Figure 1. Alternative 3′ splice site of mouse *Syngap1* inton10 induces nonsense-mediated mRNA decay

(A) Sashimi plots of isolated cortical neurons and apical neural progenitors showing *Syngap1* A3SS in embryonic day 14.5 (E14.5) mouse dorsal forebrain. The A3SS exon inclusion ratios are indicated.

(B) RNA-seq results showing that *Syngap1* A3SS was enriched in early brain development and non-neural tissues.

(C) RT-PCR results showing that the *Syngap1* A3SS was higher in the developing forebrain (76% at E12.5) and remained detectable in adulthood (5% at P40). PSI represents percent spliced in. One biological sample per lane.

(D) The *Syngap1* A3SS introduces in-frame stop codons that truncate the protein and/or induce nonsense-mediated mRNA decay.

(E) The predicted Syngap1 short protein isoform was not detectable in mouse brain lysates by western blot.

(F) The *Syngap1* A3SS transcripts were enriched in Neuro2a cells treated with cycloheximide (CHX, two biological replicates per condition, $p < 0.001$, unpaired t test).

(G) The *Syngap1* A3SS-NMD was upregulated in Neuro2a treated with two siRNAs against *Upf1* (adj.$p < 0.05$ for siRNA-1, adj.$p < 0.01$ for siRNA-2, one-way ANOVA). Two biological replicates per condition.

See also Figure S1.

SYNGAP1 A3SS-NMD is promoted by PTBP proteins

Alternative pre-mRNA splicing is regulated by RNA sequence in *cis* and splicing regulator proteins in *trans*.[31–33] We analyzed the flanking sequences of *SYNGAP1* A3SS-NMD and identified CUCUCU sequences that resemble binding motifs of PTBP1 and PTBP2 (Figure S3A). PTBP proteins are master splicing regulators in mice and humans: PTBP1 is highly expressed in neural progenitors and non-neural tissues (GTEx), and PTBP2 is expressed in immature and differentiating neurons.[22,32,34] Across different developmental stages in the human dorsal forebrain[35] (from gestational week 4 to elderly adults), *SYNGAP1* A3SS-NMD inclusion ratios showed the same decreasing trend as *PTBP1/2* mRNA levels (Figure S3B). We used shRNAs to knock down *Ptbp1* and *Ptbp2* in Neuro2a cells and found that the *Syngap1* A3SS isoform was suppressed in double knockdown samples (Figures 3A and 3B). Conversely, ectopic expression of PTBP1 in primary mouse cortical neurons decreased Syngap1 protein levels (Figures 3C and S3C). These results suggest that PTBP1 and PTBP2 suppress Syngap1 protein translation by promoting A3SS-NMD.

To determine whether *Syngap1* is a direct binding target of Ptbp proteins, we re-analyzed RNA crosslinking immunoprecipitation and sequencing (CLIP-seq) datasets of Ptbp1 in mouse embryonic stem cells (ESCs) and neural progenitor cells (NPCs),[36] and Ptbp2 CLIP-seq results in E18.5 neocortices.[37] We identified Ptbp1 and Ptbp2 CLIP tags in the *Syngap1* intron10 between the canonical and the alternative 3′ splice sites (Figure 3D). Ptbp proteins bind to CU-rich motifs and can redirect splicing by competing with U2af65/U2af2,[38] a core splicing

Please cite this article in press as: Yang et al., Upregulation of *SYNGAP1* expression in mice and human neurons by redirecting alternative splicing, Neuron (2023), https://doi.org/10.1016/j.neuron.2023.02.021

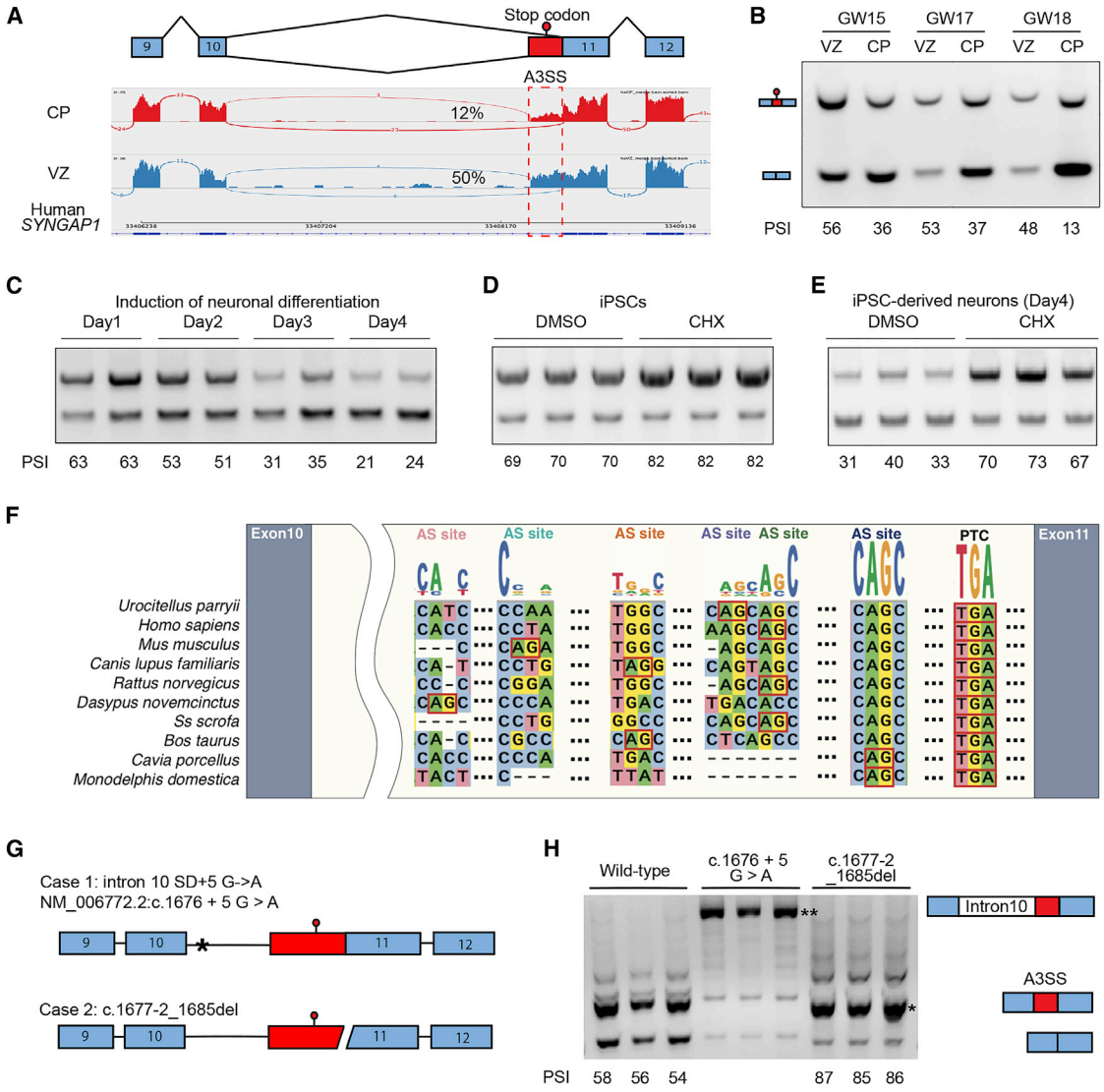

Figure 2. Human *SYNGAP1* A3SS induces nonsense-mediated mRNA decay in neural development

(A) RNA-seq results showing *SYNGAP1* A3SS in the laser microdissected cortical plate (CP) and ventricular zone (VZ) of gestational week 16 (GW16) fetal brains.[29]

(B) RT-PCR results showing that *SYNGAP1* A3SS was enriched in fetal cortical development.

(C) RT-PCR results showing that *SYNGAP1* A3SS levels significantly decreased in iPSCs during NGN1/2-induced neuronal differentiation. Two biological replicates per condition, $p < 0.001$, one-way ANOVA.

(D) *SYNGAP1* A3SS was enriched in iPSCs after CHX treatment. $p < 0.001$ by t test, three biological replicates.

(E) *SYNGAP1* A3SS ratio was increased in iPSC-derived neurons after CHX treatment. $p < 0.001$ by t test, three biological replicates.

(F) Sequence alignment showing that the premature stop codon (TGA) in *SYNGAP1* A3SS is conserved in mammals while the splice acceptor sites (AG) are variable. The AG sites were annotated according to RNA-seq results of corresponding species in NIH Genome Data Viewer.

(G and H) RT-PCR results of *SYNGAP1* mini-gene constructs (G) transfected in Neuro2a cells showing that human *SYNGAP1* intronic mutations identified in autism and ID patients led to intron 10 retention (c.1676 +5 G>A, NM_006772.2) or abnormal A3SS inclusion (c.1677 -2_1685del, $p < 0.001$ by t test, three biological replicates in H).

See also Figure S2.

factor that binds to the polypyrimidine tract for 3′ splice site recognition. We re-analyzed CLIP-seq data of U2af65 from E18.5 neocortices and found that CLIP-seq tags of U2af65 and Ptbp1 overlapped with each other on *Sygnap1* intron 10 (Figure 3D), suggesting that Ptbp1/2 may compete with U2af65 and regulate the 3′ splice site.

To identify the specific sequences and potential PTBP1 binding sites required for human *SYNGAP1* A3SS-NMD inclusion/skipping, we created a series of mini-gene constructs in which conserved DNA sequences and predicted PTBP1 binding sites were deleted (Figures 3E and S3A; STAR Methods). We identified a deep intronic element and a potential U2AF65-PTBP

Please cite this article in press as: Yang et al., Upregulation of *SYNGAP1* expression in mice and human neurons by redirecting alternative splicing, Neuron (2023), https://doi.org/10.1016/j.neuron.2023.02.021

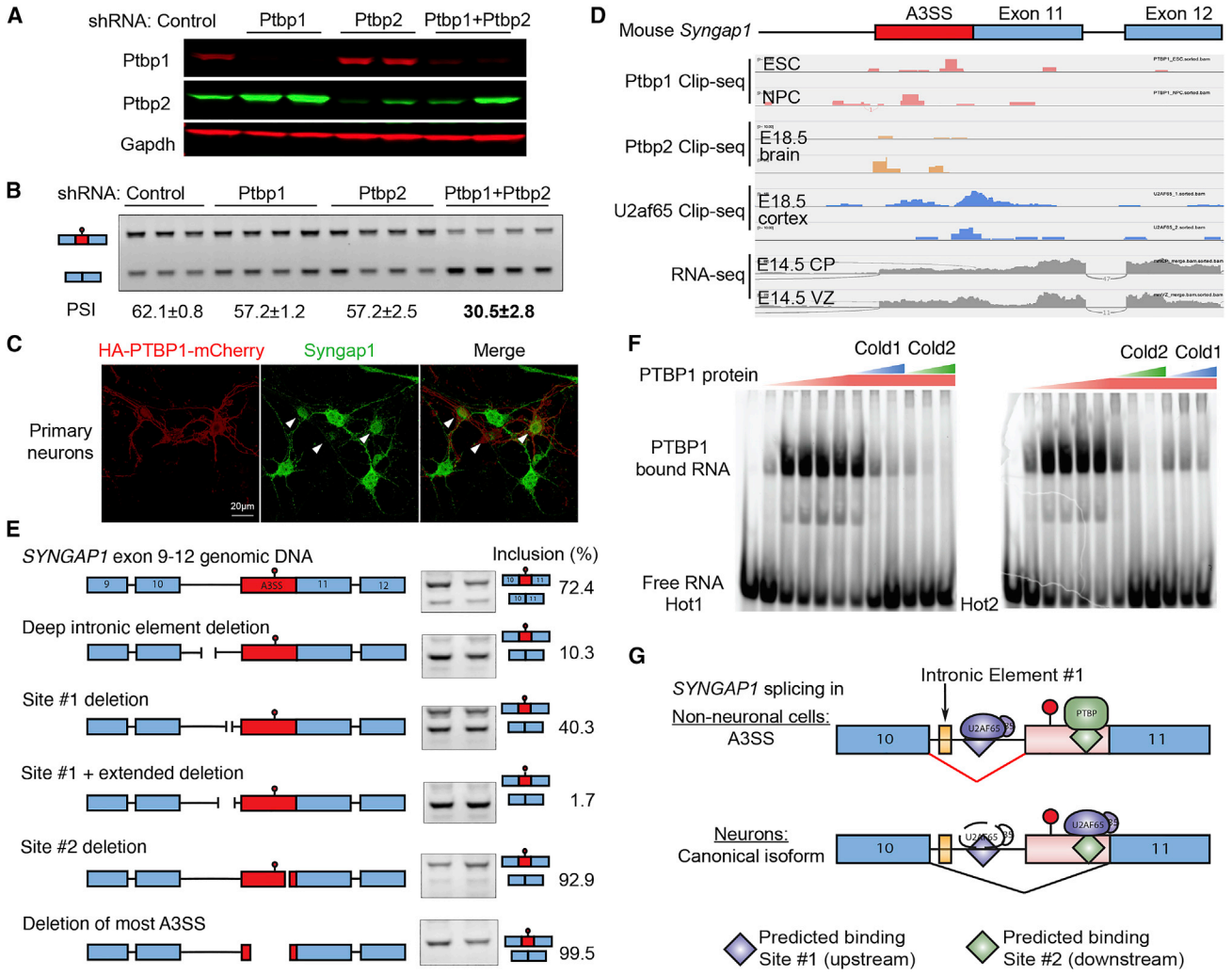

Figure 3. *SYNGAP1* A3SS-NMD is regulated by PTBP proteins

(A) Western blot results showing shRNA knockdown of Ptbp1 and Ptbp2 in Neuro2a cells. Two different shRNAs were used for each of Ptbp1 and Ptbp2.

(B) RT-PCR results showing that loss of Ptbp1/2 promoted splicing of the canonical/productive *Syngap1* isoform.

(C) Immunofluorescence staining of primary cortical neurons (DIV5) showing that ectopic expression of PTBP1 (red, mCherry) decreased Syngap1 protein level (green).

(D) CLIP-Seq analyses showing Ptbp1, Ptbp2, and U2af65 binding peaks in the A3SS region.

(E) Mini-gene constructs of the human *SYNGAP1* showing deletion of predicted splicing elements, and RT-PCR results showing their effects on A3SS insertion. Noticeably, the intronic element #1 and predicted upstream U2AF65-PTBP binding site #1 were required for A3SS inclusion; the predicted U2AF65-PTBP binding site #2 was required for canonical splicing and A3SS skipping. Two biological replicates for each condition.

(F) EMSA assay showing that PTBP1 protein had a higher affinity to the PTBP binding site #2 RNA probe.

(G) Current working model: in neural progenitors and differentiating neurons, PTBP proteins bind to site#2 in A3SS (red) and suppress the canonical/neuronal 3′ splice site; in neurons, PTBP proteins are turned down/off, and site #2 is exposed for splicing machinery (U2AF65) recognition, which promotes neuronal isoform expression.

See also Figure S3.

binding site #1 (Site #1) required for *SYNGAP1* A3SS inclusion. Additionally, we identified a fragment within the A3SS-NMD exon that is required for the canonical/productive 3′ splice site usage of *SYNGAP1* intron10. After serial deletion, we narrowed it down to a 30-base pair CUCUCU-rich polypyrimidine region, designated potential U2AF65-PTBP potential binding site #2 (Site #2, Figures 3E and S3A). Noticeably, U2AF65/U2AF2 CLIP-seq tags were concentrated near both splice acceptor sites in HEK293 cells (Figure S3A).

To examine the affinity of PTBP1 to the two predicted U2AF65-PTBP binding sites #1 and #2, we performed an electrophoretic mobility shift assay (EMSA) with PTBP1 protein and two sets of RNA probes (Figure 3F). When mixed with increasing amounts of *in vitro* translated PTBP1 protein, Cy5-labeled probes (hot)

Please cite this article in press as: Yang et al., Upregulation of *SYNGAP1* expression in mice and human neurons by redirecting alternative splicing, Neuron (2023), https://doi.org/10.1016/j.neuron.2023.02.021

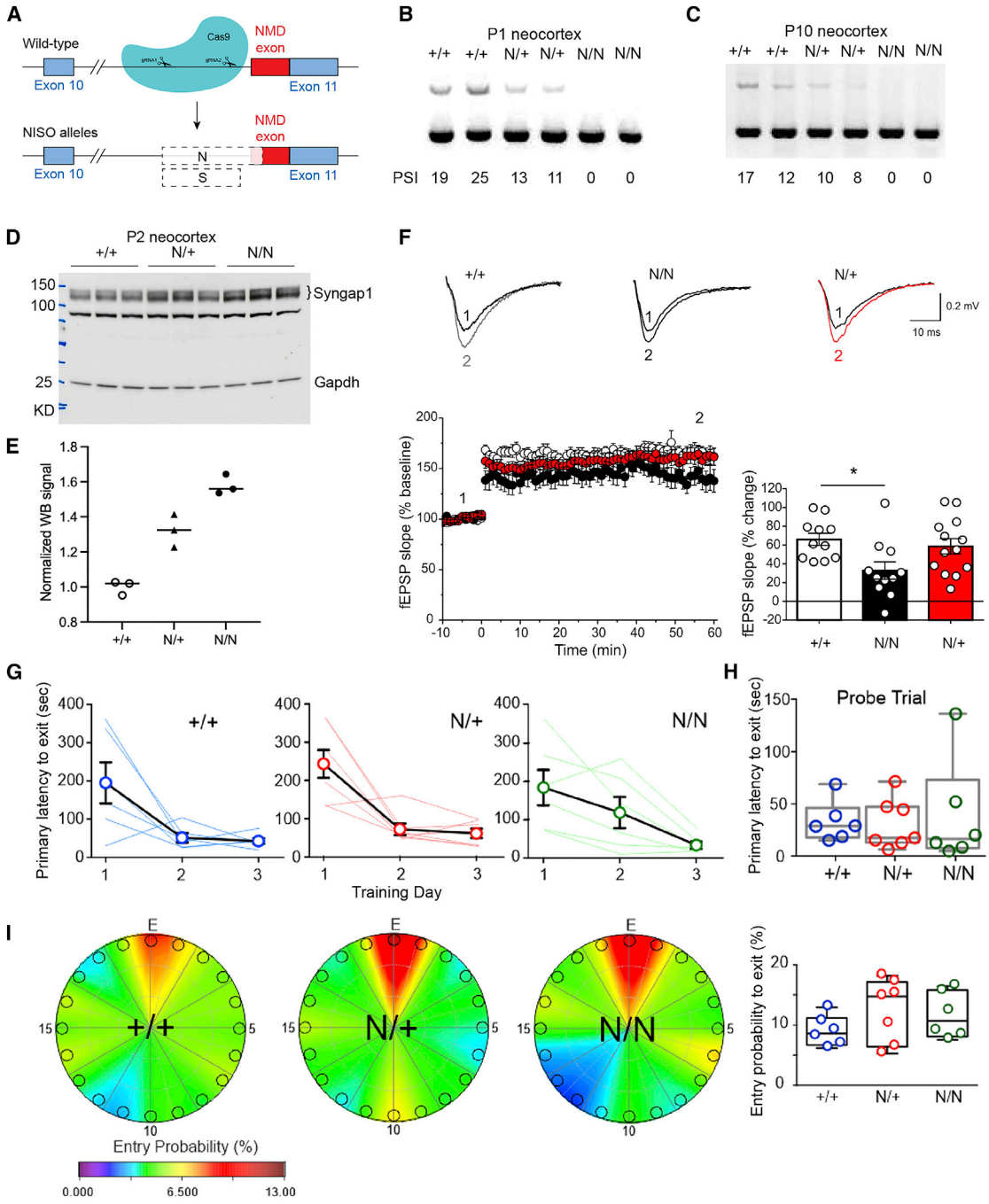

Figure 4. Genetic deletion of *Syngap1* A3SS-NMD increases Syngap1 protein in the neocortex

(A) CRISPR deletion of *Syngap1* A3SS-NMD in mice to generate the *Syngap1* NISO (N) allele (chr17:26959184-26959451, mm10) and the short NISO allele (S, chr17:26959185-26959353, mm10).

(B and C) RT-PCR results showing that *Syngap1* A3SS-NMD exon was included in wild-type controls (+/+), decreased in *Syngap1-NISO* heterozygotes (N/+), and excluded in *Syngap1-NISO* homozygotes (N/N) in P1 (B) and P10 (C) dorsal cortices.

(D) Western blot results showing Syngap1 protein levels in P2 cortices.

(E) Quantification of Syngap1 Western bot signals in (D) relative to Gapdh showing that Syngap1 levels were significantly increased in *Syngap1* N/+ (32% ± 9%, $p < 0.005$) and *Syngap1* N/N (58% ± 6%, $p < 0.001$, one-way ANOVA, Dunnett's multiple comparison test) when compared with wild type (+/+).

(F) fEPSP recordings of adult mice showing that the LTP was moderately decreased in *Syngap1* N/N. Numbers of animals and slices for each genotype were: +/+ (n = 6 animals, 11 slices), N/+ (n = 6, 13), N/N (n = 5, 11). *, adj.p = 0.0223.

(G–I) Barnes maze test results showing similar performance between wild type (+/+, n = 6) and mutants (N/+, n = 7; N/N, n = 6). (G) All genotypes show improvement in the primary latency to the exit zone over the course of training. (H) Comparisons of primary latency to the exit zone during the probe trial shows

(legend continued on next page)

Please cite this article in press as: Yang et al., Upregulation of *SYNGAP1* expression in mice and human neurons by redirecting alternative splicing, Neuron (2023), https://doi.org/10.1016/j.neuron.2023.02.021

for both Sites #1 and #2 shifted significantly; in parallel, unlabeled cold probes successfully competed with their corresponding hot probes, suggesting that PTBP1 can bind to both Sites #1 and #2 (Figure 3F). Interestingly, cold probe#2 showed more potent competition effects to hot probe#1 than cold probe#1 (Figure 3F, left), and consistently, cold probe#1 showed weaker competition than cold probe#2 to hot probe#2 (Figure 3F, right). These results suggest the model that PTBP proteins bind to the CUCUCU-rich polypyrimidine tract upstream of the canonical splice site and compete with the splicing machinery, likely through U2AF65, for the 3′ splice site definition of intron10: in neural progenitors, PTBP1 protein is expressed, binds to U2AF65-PTBP binding site #2, and suppresses the canonical/productive *SYNGAP1* splice site, whereas in neurons, PTBP proteins are turned down (Figure S3B), resulting in exposure of the *SYNGAP1* canonical splice site and increased expression of the neuronal *SYNGAP1* isoform (Figure 3G).

Deletion of *Syngap1* A3SS-NMD in mice upregulates Syngap1 protein expression

We sought to understand whether *Syngap1* A3SS-NMD is required for mouse development by genetically deleting this NMD event without affecting the protein-coding isoform (Figure 4A). Based on the results above (Figure 3E), we deleted the intronic elements and the splice acceptor site required for A3SS-NMD inclusion with CRISPR-Cas9 and created a mouse strain named *Syngap1*-NISO (standing for Neuronal ISOform, N allele, 268 bp deletion, Figures 4A and S4A). We also established a Shorter NISO allele (S allele, 160 bp deletion) where the intronic elements were deleted and the alternative 3′ splice site remained intact (Figures 4A and S4A). The *Syngap1*-NISO heterozygotes (*Syngap1* N/+, and S/+) and homozygotes (*Syngap1* N/N, and S/S) were born at expected Mendelian ratios and appeared indistinguishable from their littermates.

We confirmed the depletion of *Syngap1* A3SS-NMD intron10 in *Syngap1* N/N animals with RT-PCR amplification of the total RNA extracted from P1 and P10 neocortices (Figures 4B and 4C). Importantly, the inclusion of *Syngap1* A3SS decreased in *Syngap1*-NISO heterozygotes (N/+, Figures 4B and 4C). Similarly, the *Syngap1* A3SS significantly decreased in neocortices of P1 S/+ and S/S mutants (Figures S4A–S4C). We focused on the N allele thereafter because it led to the complete depletion of *Syngap1* A3SS-NMD in the neocortex (Figures 4B and 4C). Western blot on cortical lysates uncovered that the Syngap1 protein levels were increased by 32% ± 9% in *Syngap1* N/+ (adj.p < 0.005) and by 58% ± 6% in *Syngap1* N/N samples at P2 (adj.p < 0.001, one-way ANOVA, Dunnett's multiple comparisons) when compared with wild-type controls (+/+, Figures 4D and 4E), suggesting that one N allele can increase the protein level to 1.6 times of one wild-type allele. Syngap1 protein was also significantly increased by the *Syngap1* N/+ (96% ± 22%, adj.p = 0.018) and N/N (153% ± 25%, adj.p = 0.004) in P2 hippocampi when compared with wild type (p < 0.005, one-way ANOVA, Figures S4D and S4E). No Syngap1 protein was detected in E18.5 *Syngap1* N/+ heart or lung tissues (Figure S4G). These results indicate that suppressing *Syngap1* A3SS-NMD can increase Syngap1 protein in the developing mouse brain.

Syngap1 has been shown to suppress AMPA receptor insertion at the postsynaptic membrane; Syngap1 heterozygous knockout mice showed enhanced synaptic transmission and displayed defects in learning.[9] Our *Syngap1*-NISO allele contradicts the effects of *Syngap1* knockout alleles: the *NISO* allele increases Syngap1 protein expression, whereas the knockout allele decreases. Thus, the newly established *Syngap1-NISO* mouse model provides an opportunity to address whether the *Syngap1* A3SS-NMD is required to express LTP and influences learning and/or memory in mice.

We generated the input-output curves to evaluate basal synaptic transmission and examined the paired-pulse ratio of the field excitatory postsynaptic potentiation (fEPSP) to evaluate neurotransmitter release probability in adult wild type, *Syngap1* N/+ and N/N mice. Neither the input-output relationship nor the paired-pulse ratio was significantly different across the genotypes (Figures S4I and S4J). We measured the LTP of fEPSP in *Syngap1* N/+ and *Syngap1* N/N adult mouse hippocampi (Figure 4F). Recordings from each of the wild type (n = 8), *Syngap1* N/+ (n = 7), and *Syngap1* N/N (n = 5) genotypes showed that although LTP in wild type and *Syngap1* N/+ mutants were comparable, the magnitude of LTP was moderately but significantly reduced in *Syngap1* N/N mutants (Figure 4F). These data suggest that synaptic plasticity was affected in *Syngap1* N/N but not in *Syngap1* N/+ adults.

We next assessed performance in the Barnes maze (Figures 4G–4I) to determine spatial learning and memory abilities in *Syngap1* N/+ and N/N mice.[39] Six or more adult male animals for each genotype were trained using an abbreviated Barnes maze protocol. There were three consecutive days of training followed by a fourth-day probe trial where the exit hole was closed. The primary latency to exit decreased throughout training in all genotypes (Figure 4G). When compared with the wild type, neither *Syngap1* N/+ nor N/N mutant mice showed differences in primary latency to exit or entry probability to exit during the probe trial (Figures 4H and 4I). We also performed Rotarod assays to assess motor learning ability, and neither *Syngap1* N/+ nor *Syngap1* N/N animals showed a difference in the latency to fall when compared with wild-type mice (Figure S4H). Together, these results suggest that genetic deletion of *Syngap1* A3SS-NMD does not overtly impair spatial learning and memory or motor learning behaviors.

The NISO allele alleviates LTP and membrane excitability deficits caused by a *Syngap1* knockout allele

Increased Syngap1 protein by the *Syngap1*-NISO allele suggests that it may alleviate or rescue the *Syngap1* haploinsufficiency in mice. *Emx1-Cre* drives Cre expression in excitatory neurons in the dorsal forebrain and is sufficient to induce

that *Syngap1* mutant mice performed similarly to wild-type mice. (I) Heat maps and a boxplot showing entry probability to the exit zone and each false exit during the probe trial. *Syngap1* N/+ and *Syngap1* N/N animals were not significantly different in behavior from wild-type (+/+) mice (adj.p > 0.05). The greatest entry probability for each genotype corresponds to the exit zone.
See also Figure S4.

Please cite this article in press as: Yang et al., Upregulation of *SYNGAP1* expression in mice and human neurons by redirecting alternative splicing, Neuron (2023), https://doi.org/10.1016/j.neuron.2023.02.021

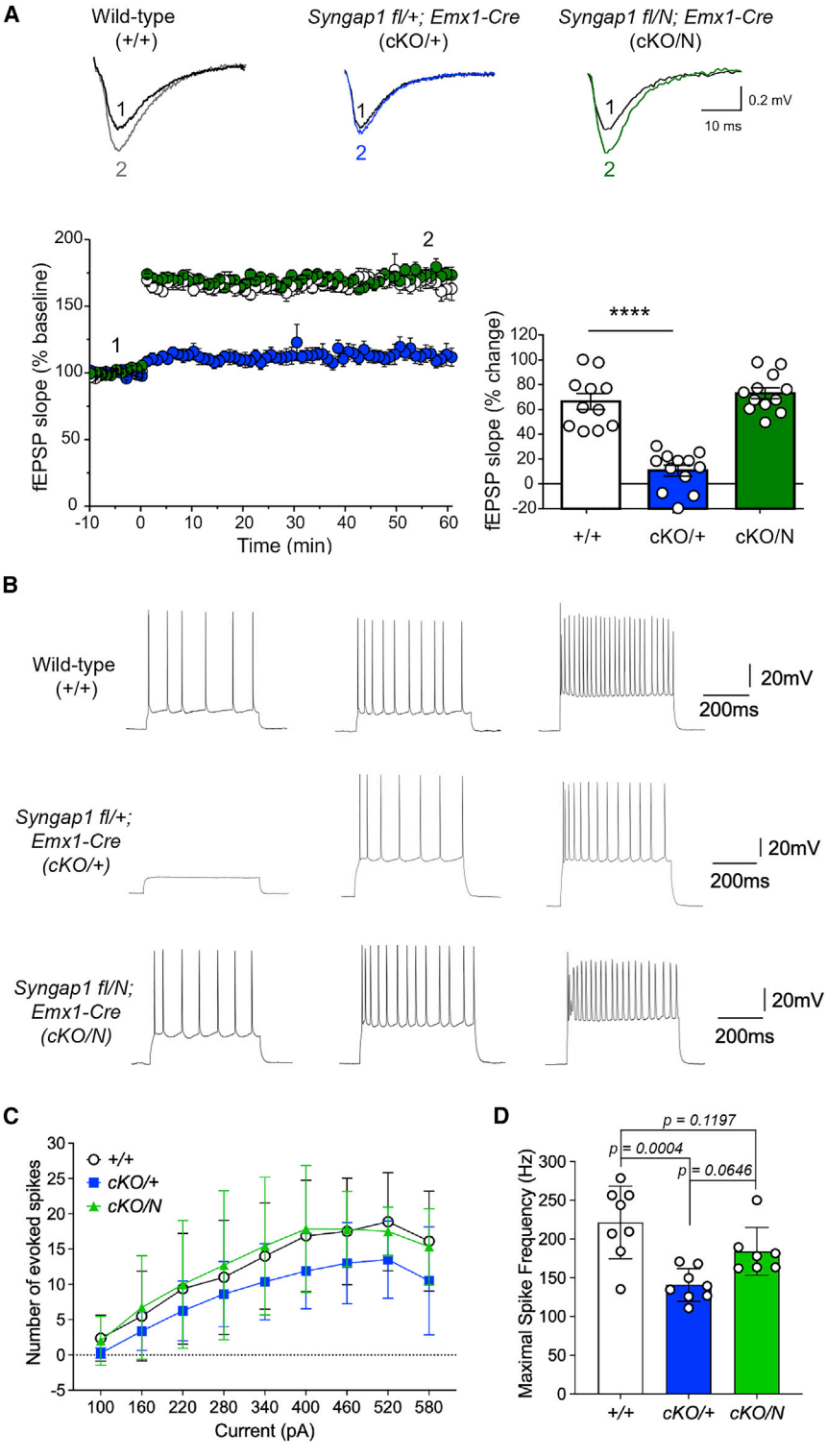

Figure 5. Genetic deletion of *Syngap1* A3SS-NMD alleviates LTP and membrane excitability deficits caused by a conditional *Syngap1* knockout allele

(A) fEPSP recordings showing that the N allele alleviates the LTP deficit in young adult *Syngap1* cKO mice. Numbers of animals and slices for each genotypes are: WT (replotted from Figure 4F), cKO/+ (n = 5, 12), and cKO/N (n = 6, 12). ****adj.p < 0.0001.

(B) Typical traces from L2/3 pyramidal neurons in S1 cortex in WT (top row), cKO/+ (middle row), and cKO/N mice (bottom row). Left to right: traces at current steps ~200 pA (left), ~400 pA (middle), and ~600 pA (right).

(C) Spike count (number of evoked spikes) per current step for WT (n = 8), cKO/+ (n = 8), and cKO/N mice (n = 7). The average ± SD is shown for all data points. p = 0.0003, F (2, 177) = 8.420 for genotype, two-way ANOVA.

(D) Dot plots showing the maximal spike frequency obtained from the same recordings. p = 0.0007 by one-way ANOVA. Each dot represents one animal. The average ± SD is shown for all data points. See also Figure S5.

Syngap1 haploinsufficient phenotypes in *Syngap1 fl/+; Emx1-Cre* (cKO/+) mice.[15] We validated the *Syngap1* conditional knockout allele (Figure S5A) in which *Syngap1* exon6-7 were floxed[9,13] and confirmed that the Syngap1 protein level decreased in adult *Syngap1* cKO/+ cortices (Figure S5B). We combined the *Syngap1-NISO* allele with the *Syngap1* floxed allele and generated *Syngap1 fl/N; Emx1-Cre* (cKO/N) and control animals (Figure S5C). We assessed basal synaptic transmission and neurotransmitter release probability in cKO/+ and cKO/N mice and did not find a significant difference in the input-output curve or paired-pulse ratio between genotypes (Figures S5E and S5F). We then evaluated LTP of the fEPSP in the hippocampi and found the LTP was impaired in *Syngap1* cKO/+ mice and rescued in *Syngap1* cKO/N animals (Figure 5A), indicating that deletion of the *Syngap1* A3SS-NMD alleviated the LTP deficits caused by the *Syngap1* knockout allele.

Syngap1 has been reported to maintain membrane excitability in L2/3 pyramidal neurons of mouse primary somatosensory cortex (S1).[16] As an independent electrophysiological test for the efficacy of our rescue strategy, we performed whole-cell patch-clamp recordings on L2/3 pyramidal neurons in the mouse S1 cortex. The current steps of increasing amplitude (500 ms) resulted in an increase in the number of evoked spikes (Figures 5B and 5C). Consistent with the earlier report, we observed a lower number of evoked spikes in the *Syngap1* cKO/+ mice (n = 8) compared with WT mice (n = 8; two-way ANOVA, genotype: $F_{2,177}$ = 8.420; p = 0.0003, pairwise adj.p = 0.0022). The difference in evoked spike output stayed constant over the range of injected current

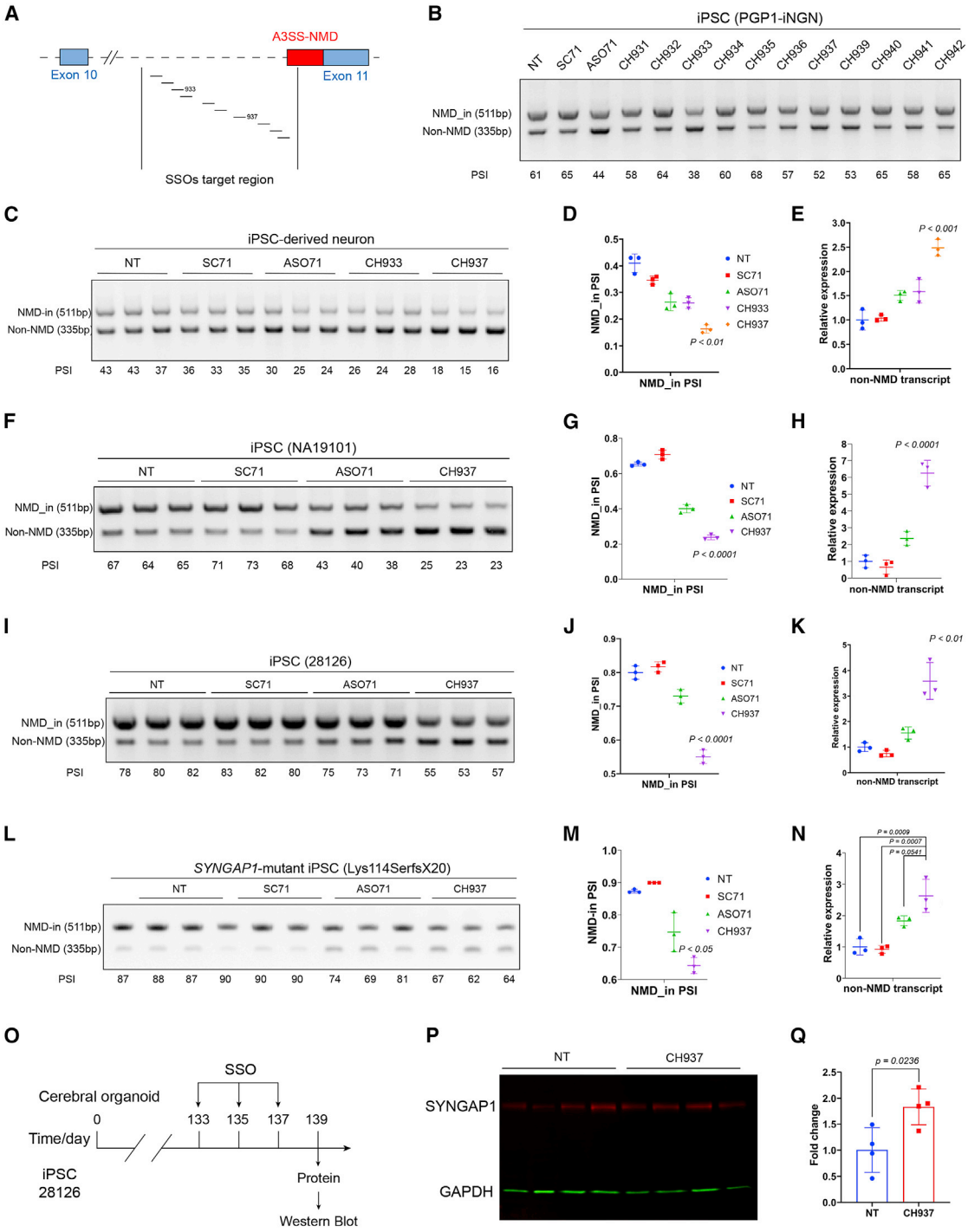

Figure 6. The lead SSO upregulates *SYNGAP1* expression in human iPSCs and iPSC-derived neurons

(A) Schematic illustration of the SSO design targeting the *SYNGAP1* A3SS.

(B) RT-PCR results showing the screening of SSOs in iPSCs (PGP1-iNGN). SC71 (scrambled control) and ASO71 were reported before.[28] One biological sample per lane.

(C–E) Identification of the lead SSO in iPSC-derived neurons. RT-PCR results (C) and quantification (D) showing that CH937 suppresses *SYNGAP1* A3SS in iPSC-derived neurons. Q-PCR results (E) showing that the productive *SYNGAP1* transcript was upregulated in CH937-treated human iPSC-derived neurons.

(F–K) The lead SSO suppresses *SYNGAP1* A3SS in two additional human iPSC lines. RT-PCR results (F and I) and quantification (G and J) showing that CH937 suppressed *SYNGAP1* A3SS in human iPSCs (NA19101 and 28126). Q-PCR results (H and K) showing that the CH937 significantly increased the productive *SYNGAP1* transcript levels in human iPSC lines.

(legend continued on next page)

Please cite this article in press as: Yang et al., Upregulation of *SYNGAP1* expression in mice and human neurons by redirecting alternative splicing, Neuron (2023), https://doi.org/10.1016/j.neuron.2023.02.021

amplitudes (genotype × current amplitude: $F_{16,117}$ = 0.1349, p > 0.9999). In *Syngap1* cKO/N mice (n = 7), the excitability deficit was restored, resulting in no significant difference when compared with WT mice (adj.p = 0.9306), but a significant difference when compared with the *Syngap1* cKO/+ mice (adj.p = 0.0011). In addition to the findings on the overall excitability, we also observed that the maximal spike firing frequency (measured from the interval of the first two evoked spikes during the current injections) was lower in *Syngap1* cKO/+ mice (n = 8) compared with WT mice (n = 8; WT: 221.43 ± 46.85 Hz; cKO/+: 140.73 ± 21.04 Hz; adj.p= 0.0004). In *Syngap1* cKO/N mice (n = 7), the higher maximal spike frequency was restored (183.99 ± 30.95 Hz; compared with WT: adj.p = 0.1197; compared with mutant: adj.p = 0.0646 by one-way ANOVA, Figure 5D). Individual action potential parameters, including overall amplitude, threshold, and width at half amplitude, did not differ between the genotypes (Figures S5G–S5I). These results indicate that deletion of the *Syngap1* A3SS-NMD alleviated the membrane excitability deficit caused by *Syngap1* haploinsufficiency in mice.

SSOs suppress *SYNGAP1* A3SS-NMD in human iPSC-derived neurons

SSOs have been successfully developed to treat neurological disorders such as spinal muscular atrophy,[26] attempted for personalized medicine,[27] and suggested to treat haploinsufficient human diseases.[40] Increased Syngap1 protein levels due to *Syngap1* A3SS deletion in mice and the conserved *SYNGAP1* A3SS in human brains led us to determine whether the *SYNGAP1* productive isoform can be upregulated in human cells through SSO-mediated suppression of *SYNGAP1* A3SS-NMD. SSOs with 2'-O-methoxyethyl (2′-MOE) chemistry have been successfully developed to redirect splicing, manipulate gene expression, and treat diseases.[41] To identify SSOs that suppress human *SYNGAP1* A3SS-NMD, we performed a rationale design by targeting the following sequences (Figure 6A): (1) critical splice elements identified through serial deletion of the human *SYNGAP1* mini-gene (Figure 3), (2) predicted splicing regulatory sequences such as branch points,[42] (3) predicted stem-loop structures and conserved sequences that overlap with experimentally identified splice elements (Figures 6A and S6A).

We synthesized eleven SSOs using a phosphorothioate backbone with 2′-MOE modified residues and tested them in human iPSCs (Figures 6A and 6B). SSOs CH933 and CH937 most efficiently suppressed A3SS-NMD inclusion in a human iPSC line (PGP1-iNGN, Figures 6B and S6A–S6C). We delivered SSOs CH933 and CH937, a scrambled control, and a previously reported ASO71[28] into human iPSC-derived neurons and found that CH937 was the most effective in decreasing the A3SS-NMD inclusion (Figures 6C and 6D). We further measured the productive/functional *SYNGAP1* transcript using Q-PCR primers specific to the non-NMD isoform, and CH937 induced a 2.5-fold increase of functional *SYNGAP1* mRNA (Tukey's multiple comparisons tests, adj.p < 0.001, Figure 6E). By contrast, the ASO71 developed in HEK293 cells was less efficient in upregulating *SYNGAP1* transcript in human iPSC-derived neurons (1.5 fold, adj.p = 0.029, Figure 6E). These results indicate that the lead SSO CH937 can effectively suppress human A3SS-NMD and increase the alternative *SYNGAP1* isoform in human iPSCs and iPSC-derived neurons.

We further examined the effects of the SSO CH937 in two additional control human iPSC lines (NA19101 and 28126) and confirmed that CH937 was more effective than ASO71 in decreasing the *SYNGAP1* A3SS-NMD inclusion (Figures 6F–6K). Importantly, CH937 significantly increased the functional *SYNGAP1* transcript to 6.3-fold and 3.6-fold of non-treated controls in NA19101 and 28126, respectively (Figures 6H and 6K). Next, we delivered CH937 to a *SYNGAP1* patient-derived iPSC line harboring a heterozygous frameshift mutation (Lys114SerfsX20) and found that the SSO CH937 decreased *SYNGAP1* A3SS-NMD inclusion (Figures 6L and 6M) and significantly increased functional *SYNGAP1* transcript to 2.6-fold of non-treated controls (Figure 6N). These results support that the lead SSO CH937 can effectively suppress the *SYNGAP1* A3SS-NMD and increase functional *SYNGAP1* isoform levels in *SYNGAP1* patient-derived iPSCs.

To determine whether suppressing the *SYNGAP1* A3SS-NMD can upregulate SYNGAP1 protein, we evaluated the effects of SSO CH937 in iPSC-derived brain organoids. Cerebral organoids were induced from human iPSCs (28,126) following an established protocol,[43] transfected with CH937 at post-induction days 133, 135, and 137, and harvested at day 139 for protein analysis (Figures 6O and 6P). CH937 significantly increased SYNGAP1 protein when compared with control organoids (83% ± 28%, p < 0.05 by unpaired t test). We further tested SSO CH937 in cerebral organoids derived from another iPSC line (21,792) at post-induction day 174 and again observed increased SYNGAP1 protein when compared with control oligonucleotides (Figures S6E–S6G, increased by 51% ± 10%, adj.p = 0.0051 by one-way ANOVA). These results suggest that the SSO CH937 can upregulate *SYNGAP1* protein in human iPSC-derived cerebral organoids.

DISCUSSION

Alternative splicing coupled with NMD selectively removes unproductive transcripts and has been reported to regulate the expression of neuronal genes.[21–23,44] The therapeutic potential of targeting AS-NMD with SSOs has evoked unprecedented enthusiasm, and SSO screens in cultured cells have been reported in recent studies.[28,40,45] However, whether it is safe to target naturally occurring AS-NMD for therapy remains a crucial question. Specifically, we need to understand whether such an

(L–N) The lead SSO suppresses *SYNGAP1* A3SS-NMD in *SYNGAP1* patient-derived iPSCs. RT-PCR results (L) and quantification (M) showing that CH937 suppressed *SYNGAP1* A3SS in *SYNGAP1* patient-derived iPSCs (333del, Lys114SerfsX20). Q-PCR results (N) showing that the CH937 significantly increased the productive *SYNGAP1* mRNA level.

(O–Q) Application of CH937 to human iPSC-derived cerebral organoids (O) led to increased SYNGAP1 protein expression (83% ± 28%, P and Q). p < 0.05 by unpaired t test.

See also Figure S6.

Please cite this article in press as: Yang et al., Upregulation of *SYNGAP1* expression in mice and human neurons by redirecting alternative splicing, Neuron (2023), https://doi.org/10.1016/j.neuron.2023.02.021

AS-NMD exon is required for normal organismal functions and whether it is safe to suppress or completely block such an AS-NMD exon *in vivo*.

Since presenting our *SYNGAP1* A3SS-NMD results at the 2019 Society for Neuroscience meeting (Chicago), we have further explored the function and therapeutic potential of the *SYNGAP1* A3SS using mouse genetics and human iPSCs. Syngap1 is a synaptic protein barely detected in non-neuronal tissues.[4] By contrast, the *SYNGAP1* transcript is detectable in non-neural tissues in mice and in humans (Figure 1 and GTEx), where the *Syngap1* A3SS-NMD inclusion is nearly constitutive (Figure 1B). These observations suggest that A3SS-NMD provides an orthogonal mechanism in non-neuronal cells to suppress excess or leaky SYNGAP1 expression that would waste cellular resources and interfere with Ras signaling. Our results support that heterozygous genetic deletion of *Syngap1* A3SS in mice upregulated SYNGAP1 protein during brain development. Although homozygous deletion of mouse *Syngap1* A3SS led to a modest reduction in the magnitude of LTP, it did not overtly impact behavioral performance in the Barnes maze or Rotarod assays. We were unable to detect Syngap1 protein in E18.5 heart or lung tissues from *Syngap1* N/+ animals (Figure S4G), and there was no significant cortical neurogenesis defect in *Syngap1* N/N mice (Figure S4F). Our results suggest that the *Syngap1* A3SS is moderately required during neural development, and its functions in non-neural tissues remain to be further explored.

Heterozygous deletion of mouse *Syngap1* A3SS alleviated the LTP deficits caused by a heterozygous *Syngap1* knockout allele, suggesting that suppressing A3SS-NMD may alleviate *Syngap1* haploinsufficiency *in vivo* (Figure 5). A previous study has reported that *Syngap1* heterozygous deletion reduced membrane excitability, as tested via the trains of injected current pulses of increasing amplitude.[16] Here, we adapted this experimental protocol to capture a cell-autonomous physiological parameter that differs from LTP. We found that the maximal spike firing frequency–which, because of spike frequency adaptation occurs at the beginning of the current pulse[46] and is typically determined from the interval of the first two spikes—was lower in *Syngap1* heterozygous knockouts than in wild-type mice. Both the general excitability and the maximal spike frequency defects were alleviated by the heterozygous deletion of *Syngap1* A3SS.

Furthermore, our lead SSO CH937 suppressed *SYNGAP1* A3SS in human iPSCs and iPSC-derived neurons and significantly increased the functional *SYNGAP1* isoform. The SSO CH937 also increased SYNGAP1 protein expression in cerebral organoids induced from two different human iPSC lines. Despite these encouraging results, several key questions remain to be further addressed: (1) it is important to understand at what time and in which brain regions the rescuing effects of *Syngap1* upregulation are sufficient to rescue haploinsufficiency. Specifically, it is critical to understand whether deleting or suppressing the A3SS-NMD exon at postnatal stages can rescue the heterozygous knockout allele. It is equally important to systematically characterize neural circuits and mouse behaviors because *SYNGAP1* patients display pleiotropic symptoms.[7] (2) It is important to understand whether the SSO can effectively upregulate Syngap1 protein *in vivo* and rescue the heterozygous knockout mouse. Although the *Syngap1 NISO* mouse model and the lead SSO CH937 suggest that *SYNGAP1* A3SS is a promising target, rigorous further *in vivo* studies are required to understand its therapeutic potential fully.

SYNGAP1 protein directly interacts with PSD-95 in the post-synaptic density, and remarkably, both genes undergo unproductive splicing that is promoted by PTBP1 and PTBP2 in early neural development. Although PTBP proteins promote *SYNGAP1* A3SS-NMD inclusion, they suppress the inclusion of a coding exon in *PSD-95/DLG4* and lead to NMD.[44] Previous studies showed that protein levels of SYNGAP1 and PSD-95 exhibit a near stoichiometric ratio in the PSD and the appropriate protein ratio is critical for the formation of SYNGAP1-PSD-95 liquid-like droplets.[47] Strikingly, two AS-NMD events are co-regulated by the PTBP1/2 proteins for equilibrated protein expression. *De novo* mutations in *PSD-95* have been reported to cause synaptopathy.[48] It is interesting to speculate on the functions of the *PSD-95* AS-NMD exon and its potential as a therapeutic target.

Hundreds of genes have been reported to undergo AS-NMD during cortical development, and chromatin regulators were highly enriched.[21] The AS-NMD exons are regulated by splicing regulators, and mutations in the host genes are frequently associated with neurodevelopmental disorders such as autism and epilepsy.[22,23,31,32,33,45,49,50] Although AS-NMD exons have been reported as promising targets to treat diseases such as the Dravet Syndrome,[40] the biological functions of such AS-NMD events are undetermined. Furthermore, the dosage effect of their host genes requires rigorous studies in animal models and human neurons to fully explore their therapeutic potential. Genetic studies of AS-NMD exons will illuminate their organismal functions and further the development of therapeutic targets and strategies.

STAR★METHODS

Detailed methods are provided in the online version of this paper and include the following:

- KEY RESOURCES TABLE
- RESOURCE AVAILABILITY
  - Lead contact
  - Materials availability
  - Data and code availability
- EXPERIMENTAL MODEL AND SUBJECT DETAILS
  - Animals
  - Primary cell culture
  - Human iPSCs
  - Cerebral organoids
  - Fetal cortical tissue
- METHOD DETAILS
  - Molecular cloning
  - RT-PCR and Western blot
  - EMSA
  - Mouse behavioral tests
  - fEPSP recordings
  - Whole-cell patch-clamp recordings

- Primary neuron transfection and immunostaining
- Splice-switching oligonucleotides

● QUANTIFICATION AND STATISTICAL ANALYSIS

SUPPLEMENTAL INFORMATION

Supplemental information can be found online at https://doi.org/10.1016/j.neuron.2023.02.021.

ACKNOWLEDGMENTS

The authors would like to thank Profs. Jonathan P. Staley (UChicago), Xiaoxi Zhuang (UChicago), Francois Spitz (UChicago), Yoav Gilad (UChicago), and Benoit Laurent (Université de Sherbrooke) for sharing reagents and valuable comments; colleagues in the Department of Human Genetics, the Neuroscience Institute, and the Genomics Core at UChicago for supporting this work; and Zhang lab members for technical support and in-depth discussions. R.S.Z. was supported by the Quad Undergraduate Research Scholarship. C.A.P. was supported by the 2022 DENDRITES Leadership Alliance Program. A.A.-C., A.P., and A.J.G. were supported by a grant from the NINDS (R01 NS107421) to A.J.G. The generation of Syngap1-*NISO* mice was supported by the National Center for Advancing Translational Sciences (NCATS) of the National Institutes of Health (NIH) through grant number 5UL1TR002389-04 that funds the Institute for Translational Medicine (ITM). This work was supported by grants from the NIMH (K01 MH109747 and R01 MH130594) and the NIGMS (DP2 GM137423) to X.Z.

AUTHOR CONTRIBUTIONS

R.Y., X.F., K.H., R.Z., C.Q., R.S.Z., N.W., M.A.N., and X.Z. performed molecular, cellular, and organismal experiments and analyzed data. A.A.-C., R.M.M., A.P., and C.A.P. performed electrophysiology experiments and analyzed the results under the guidance of C.H. and A.J.G. X.Z. conceived the framework and supervised this study. R.Y., X.F., and X.Z. wrote the manuscript with input from all co-authors.

DECLARATION OF INTERESTS

A provisional patent on splice-switching oligonucleotides described in this study has been filed on behalf of X.Z. and R.Y.

Received: August 15, 2022
Revised: December 20, 2022
Accepted: February 13, 2023
Published: March 13, 2023

REFERENCES

1. Zoghbi, H.Y., and Bear, M.F. (2012). Synaptic dysfunction in neurodevelopmental disorders associated with autism and intellectual disabilities. Cold Spring Harb. Perspect. Biol. *4*, a009886. https://doi.org/10.1101/cshperspect.a009886.
2. Südhof, T.C. (2018). Towards an understanding of synapse formation. Neuron *100*, 276–293. https://doi.org/10.1016/j.neuron.2018.09.040.
3. Chen, H.J., Rojas-Soto, M., Oguni, A., and Kennedy, M.B. (1998). A synaptic Ras-GTPase activating protein (p135 SynGAP) inhibited by CaM kinase II. Neuron *20*, 895–904.
4. Kim, J.H., Liao, D., Lau, L.F., and Huganir, R.L. (1998). SynGAP: a synaptic rasgap that associates with the PSD-95/SAP90 protein family. Neuron *20*, 683–691.
5. Hamdan, F.F., Gauthier, J., Spiegelman, D., Noreau, A., Yang, Y., Pellerin, S., Dobrzeniecka, S., Côté, M., Perreau-Linck, E., Carmant, L., et al. (2009). Mutations in SYNGAP1 in autosomal nonsyndromic mental retardation. N. Engl. J. Med. *360*, 599–605. https://doi.org/10.1056/NEJMoa0805392.
6. Satterstrom, F.K., Kosmicki, J.A., Wang, J., Breen, M.S., De Rubeis, S., An, J.Y., Peng, M., Collins, R., Grove, J., Klei, L., et al. (2020). Large-scale exome sequencing study implicates both developmental and functional changes in the neurobiology of autism. Cell *180*. 568–584.e23. https://doi.org/10.1016/j.cell.2019.12.036.
7. Vlaskamp, D.R.M., Shaw, B.J., Burgess, R., Mei, D., Montomoli, M., Xie, H., Myers, C.T., Bennett, M.F., XiangWei, W., Williams, D., et al. (2019). SYNGAP1 encephalopathy: a distinctive generalized developmental and epileptic encephalopathy. Neurology *92*, e96–e107. https://doi.org/10.1212/WNL.0000000000006729.
8. Berryer, M.H., Hamdan, F.F., Klitten, L.L., Møller, R.S., Carmant, L., Schwartzentruber, J., Patry, L., Dobrzeniecka, S., Rochefort, D., Neugnot-Cerioli, M., et al. (2013). Mutations in SYNGAP1 cause intellectual disability, autism, and a specific form of epilepsy by inducing haploinsufficiency. Hum. Mutat. *34*, 385–394. https://doi.org/10.1002/humu.22248.
9. Clement, J.P., Aceti, M., Creson, T.K., Ozkan, E.D., Shi, Y., Reish, N.J., Almonte, A.G., Miller, B.H., Wiltgen, B.J., Miller, C.A., et al. (2012). Pathogenic SYNGAP1 mutations impair cognitive development by disrupting maturation of dendritic spine synapses. Cell *151*, 709–723. https://doi.org/10.1016/j.cell.2012.08.045.
10. Kim, M.J., Dunah, A.W., Wang, Y.T., and Sheng, M. (2005). Differential roles of NR2A- and NR2B-containing NMDA receptors in Ras-ERK signaling and AMPA receptor trafficking. Neuron *46*, 745–760. https://doi.org/10.1016/j.neuron.2005.04.031.
11. Rumbaugh, G., Adams, J.P., Kim, J.H., and Huganir, R.L. (2006). SynGAP regulates synaptic strength and mitogen-activated protein kinases in cultured neurons. Proc. Natl. Acad. Sci. USA *103*, 4344–4351. https://doi.org/10.1073/pnas.0600084103.
12. Araki, Y., Zeng, M., Zhang, M., and Huganir, R.L. (2015). Rapid dispersion of SynGAP from synaptic spines triggers AMPA receptor insertion and spine enlargement during LTP. Neuron *85*, 173–189. https://doi.org/10.1016/j.neuron.2014.12.023.
13. Komiyama, N.H., Watabe, A.M., Carlisle, H.J., Porter, K., Charlesworth, P., Monti, J., Strathdee, D.J., O'Carroll, C.M., Martin, S.J., Morris, R.G., et al. (2002). SynGAP regulates ERK/MAPK signaling, synaptic plasticity, and learning in the complex with postsynaptic density 95 and NMDA receptor. J. Neurosci. *22*, 9721–9732.
14. Kim, J.H., Lee, H.K., Takamiya, K., and Huganir, R.L. (2003). The role of synaptic GTPase-activating protein in neuronal development and synaptic plasticity. J. Neurosci. *23*, 1119–1124.
15. Ozkan, E.D., Creson, T.K., Kramár, E.A., Rojas, C., Seese, R.R., Babyan, A.H., Shi, Y., Lucero, R., Xu, X., Noebels, J.L., et al. (2014). Reduced cognition in Syngap1 mutants is caused by isolated damage within developing forebrain excitatory neurons. Neuron *82*, 1317–1333. https://doi.org/10.1016/j.neuron.2014.05.015.
16. Michaelson, S.D., Ozkan, E.D., Aceti, M., Maity, S., Llamosas, N., Weldon, M., Mizrachi, E., Vaissiere, T., Gaffield, M.A., Christie, J.M., et al. (2018). SYNGAP1 heterozygosity disrupts sensory processing by reducing touch-related activity within somatosensory cortex circuits. Nat. Neurosci. *21*, 1–13. https://doi.org/10.1038/s41593-018-0268-0.
17. Berryer, M.H., Chattopadhyaya, B., Xing, P., Riebe, I., Bosoi, C., Sanon, N., Antoine-Bertrand, J., Lévesque, M., Avoli, M., Hamdan, F.F., et al. (2016). Decrease of SYNGAP1 in GABAergic cells impairs inhibitory synapse connectivity, synaptic inhibition and cognitive function. Nat. Commun. *7*, 13340. https://doi.org/10.1038/ncomms13340.
18. Creson, T.K., Rojas, C., Hwaun, E., Vaissiere, T., Kilinc, M., Jimenez-Gomez, A., Holder, J.L., Jr., Tang, J., Colgin, L.L., Miller, C.A., et al. (2019). Re-expression of SynGAP protein in adulthood improves translatable measures of brain function and behavior. eLife *8*, e46752. https://doi.org/10.7554/eLife.46752.
19. Lareau, L.F., Inada, M., Green, R.E., Wengrod, J.C., and Brenner, S.E. (2007). Unproductive splicing of SR genes associated with highly conserved and ultraconserved DNA elements. Nature *446*, 926–929. https://doi.org/10.1038/nature05676.

Please cite this article in press as: Yang et al., Upregulation of *SYNGAP1* expression in mice and human neurons by redirecting alternative splicing, Neuron (2023), https://doi.org/10.1016/j.neuron.2023.02.021

20. Black, D.L. (2003). Mechanisms of alternative pre-messenger RNA splicing. Annu. Rev. Biochem. *72*, 291–336. https://doi.org/10.1146/annurev.biochem.72.121801.161720.

21. Yan, Q., Weyn-Vanhentenryck, S.M., Wu, J., Sloan, S.A., Zhang, Y., Chen, K., Wu, J.Q., Barres, B.A., and Zhang, C. (2015). Systematic discovery of regulated and conserved alternative exons in the mammalian brain reveals NMD modulating chromatin regulators. Proc. Natl. Acad. Sci. USA *112*, 3445–3450. https://doi.org/10.1073/pnas.1502849112.

22. Zhang, X., Chen, M.H., Wu, X., Kodani, A., Fan, J., Doan, R., Ozawa, M., Ma, J., Yoshida, N., Reiter, J.F., et al. (2016). Cell-type-specific alternative splicing governs cell fate in the developing cerebral cortex. Cell *166*. 1147–1162.e15. https://doi.org/10.1016/j.cell.2016.07.025.

23. Carvill, G.L., Engel, K.L., Ramamurthy, A., Cochran, J.N., Roovers, J., Stamberger, H., Lim, N., Schneider, A.L., Hollingsworth, G., Holder, D.H., et al. (2018). Aberrant inclusion of a poison exon causes Dravet syndrome and related SCN1A-associated genetic epilepsies. Am. J. Hum. Genet. *103*, 1022–1029. https://doi.org/10.1016/j.ajhg.2018.10.023.

24. Lin, L., Zhang, M., Stoilov, P., Chen, L., and Zheng, S. (2020). Developmental attenuation of neuronal apoptosis by neural-specific splicing of Bak1 microexon. Neuron *107*. 1180–1196.e8. https://doi.org/10.1016/j.neuron.2020.06.036.

25. Hua, Y., Sahashi, K., Rigo, F., Hung, G., Horev, G., Bennett, C.F., and Krainer, A.R. (2011). Peripheral SMN restoration is essential for long-term rescue of a severe spinal muscular atrophy mouse model. Nature *478*, 123–126. https://doi.org/10.1038/nature10485.

26. Finkel, R.S., Mercuri, E., Darras, B.T., Connolly, A.M., Kuntz, N.L., Kirschner, J., Chiriboga, C.A., Saito, K., Servais, L., Tizzano, E., et al. (2017). Nusinersen versus sham control in infantile-onset spinal muscular atrophy. N. Engl. J. Med. *377*, 1723–1732. https://doi.org/10.1056/NEJMoa1702752.

27. Kim, J., Hu, C., Moufawad El Achkar, C., Black, L.E., Douville, J., Larson, A., Pendergast, M.K., Goldkind, S.F., Lee, E.A., Kuniholm, A., et al. (2019). Patient-customized oligonucleotide therapy for a rare genetic disease. N. Engl. J. Med. *381*, 1644–1652. https://doi.org/10.1056/NEJMoa1813279.

28. Lim, K.H., Han, Z., Jeon, H.Y., Kach, J., Jing, E., Weyn-Vanhentenryck, S., Downs, M., Corrionero, A., Oh, R., Scharner, J., et al. (2020). Antisense oligonucleotide modulation of non-productive alternative splicing upregulates gene expression. Nat. Commun. *11*, 3501. https://doi.org/10.1038/s41467-020-17093-9.

29. Camp, J.G., Badsha, F., Florio, M., Kanton, S., Gerber, T., Wilsch-Bräuninger, M., Lewitus, E., Sykes, A., Hevers, W., Lancaster, M., et al. (2015). Human cerebral organoids recapitulate gene expression programs of fetal neocortex development. Proc. Natl. Acad. Sci. USA *112*, 15672–15677. https://doi.org/10.1073/pnas.1520760112.

30. Prchalova, D., Havlovicova, M., Sterbova, K., Stranecky, V., Hancarova, M., and Sedlacek, Z. (2017). Analysis of 31-year-old patient with SYNGAP1 gene defect points to importance of variants in broader splice regions and reveals developmental trajectory of SYNGAP1-associated phenotype: case report. BMC Med. Genet. *18*, 62. https://doi.org/10.1186/s12881-017-0425-4.

31. Darnell, R.B. (2013). RNA protein interaction in neurons. Annu. Rev. Neurosci. *36*, 243–270. https://doi.org/10.1146/annurev-neuro-062912-114322.

32. Vuong, C.K., Black, D.L., and Zheng, S. (2016). The neurogenetics of alternative splicing. Nat. Rev. Neurosci. *17*, 265–281. https://doi.org/10.1038/nrn.2016.27.

33. Raj, B., and Blencowe, B.J. (2015). Alternative splicing in the mammalian nervous system: recent insights into mechanisms and functional roles. Neuron *87*, 14–27. https://doi.org/10.1016/j.neuron.2015.05.004.

34. Boutz, P.L., Stoilov, P., Li, Q., Lin, C.H., Chawla, G., Ostrow, K., Shiue, L., Ares, M., Jr., and Black, D.L. (2007). A post-transcriptional regulatory switch in polypyrimidine tract-binding proteins reprograms alternative splicing in developing neurons. Genes Dev. *21*, 1636–1652. https://doi.org/10.1101/gad.1558107.

35. Lindsay, S.J., Xu, Y., Lisgo, S.N., Harkin, L.F., Copp, A.J., Gerrelli, D., Clowry, G.J., Talbot, A., Keogh, M.J., Coxhead, J., et al. (2016). HDBR expression: A unique resource for global and individual gene expression studies during early human brain development. Front. Neuroanat. *10*, 86. https://doi.org/10.3389/fnana.2016.00086.

36. Linares, A.J., Lin, C.H., Damianov, A., Adams, K.L., Novitch, B.G., and Black, D.L. (2015). The splicing regulator PTBP1 controls the activity of the transcription factor Pbx1 during neuronal differentiation. eLife *4*, e09268. https://doi.org/10.7554/eLife.09268.

37. Licatalosi, D.D., Yano, M., Fak, J.J., Mele, A., Grabinski, S.E., Zhang, C., and Darnell, R.B. (2012). Ptbp2 represses adult-specific splicing to regulate the generation of neuronal precursors in the embryonic brain. Genes Dev. *26*, 1626–1642. https://doi.org/10.1101/gad.191338.112.

38. Saulière, J., Sureau, A., Expert-Bezançon, A., and Marie, J. (2006). The polypyrimidine tract binding protein (PTB) represses splicing of exon 6B from the beta-tropomyosin pre-mRNA by directly interfering with the binding of the U2AF65 subunit. Mol. Cell. Biol. *26*, 8755–8769. https://doi.org/10.1128/MCB.00893-06.

39. Pitts, M.W. (2018). Barnes maze procedure for spatial learning and memory in mice. Bio Protoc. *8*, 8. https://doi.org/10.21769/bioprotoc.2744.

40. Han, Z., Chen, C., Christiansen, A., Ji, S., Lin, Q., Anumonwo, C., Liu, C., Leiser, S.C., Meena, A., Aznarez, I., et al. (2020). Antisense oligonucleotides increase Scn1a expression and reduce seizures and SUDEP incidence in a mouse model of Dravet syndrome. Sci. Transl. Med. *12*, eaaz6100. https://doi.org/10.1126/scitranslmed.aaz6100.

41. Kole, R., Krainer, A.R., and Altman, S. (2012). RNA therapeutics: beyond RNA interference and antisense oligonucleotides. Nat. Rev. Drug Discov. *11*, 125–140. https://doi.org/10.1038/nrd3625.

42. Zeng, Y., Fair, B.J., Zeng, H., Krishnamohan, A., Hou, Y., Hall, J.M., Ruthenburg, A.J., Li, Y.I., and Staley, J.P. (2022). Profiling lariat intermediates reveals genetic determinants of early and late co-transcriptional splicing. Mol. Cell. *82*, 4681–4699. https://doi.org/10.1016/j.molcel.2022.11.004.

43. Yoon, S.J., Elahi, L.S., Paşca, A.M., Marton, R.M., Gordon, A., Revah, O., Miura, Y., Walczak, E.M., Holdgate, G.M., Fan, H.C., et al. (2019). Reliability of human cortical organoid generation. Nat. Methods *16*, 75–78. https://doi.org/10.1038/s41592-018-0255-0.

44. Zheng, S., Gray, E.E., Chawla, G., Porse, B.T., O'Dell, T.J., and Black, D.L. (2012). PSD-95 is post-transcriptionally repressed during early neural development by PTBP1 and PTBP2. Nat. Neurosci. *15*, 381–388. https://doi.org/10.1038/nn.3026.

45. Dawicki-McKenna, J.M.F., A.J., Waxman, E.A., Cheng, C., Amado, D.A., Ranum, P.T., Lea Dungan, V., A.B., Heller, E.A., et al. (2022). Mapping PTBP splicing in human brain identifies targets for therapeutic splice switching including SYNGAP1. https://doi.org/10.1101/2022.07.15.500219.

46. Gill, D.F., and Hansel, C. (2020). Muscarinic modulation of SK2-type K(+) channels promotes intrinsic plasticity in L2/3 pyramidal neurons of the mouse primary somatosensory cortex. eNeuro *7*. ENEURO.0453-19.2020. https://doi.org/10.1523/ENEURO.0453-19.2020.

47. Zeng, M., Shang, Y., Araki, Y., Guo, T., Huganir, R.L., and Zhang, M. (2016). Phase transition in postsynaptic densities underlies formation of synaptic complexes and synaptic plasticity. Cell *166*. 1163–1175.e12. https://doi.org/10.1016/j.cell.2016.07.008.

48. Rodríguez-Palmero, A., Boerrigter, M.M., Gómez-Andrés, D., Aldinger, K.A., Marcos-Alcalde, Í., Popp, B., Everman, D.B., Lovgren, A.K., Arpin, S., Bahrambeigi, V., et al. (2021). DLG4-related synaptopathy: a new rare brain disorder. Genet. Med. *23*, 888–899. https://doi.org/10.1038/s41436-020-01075-9.

Please cite this article in press as: Yang et al., Upregulation of *SYNGAP1* expression in mice and human neurons by redirecting alternative splicing, Neuron (2023), https://doi.org/10.1016/j.neuron.2023.02.021

49. Weyn-Vanhentenryck, S.M., Mele, A., Yan, Q., Sun, S., Farny, N., Zhang, Z., Xue, C., Herre, M., Silver, P.A., Zhang, M.Q., et al. (2014). HITS-CLIP and integrative modeling define the Rbfox splicing-regulatory network linked to brain development and autism. Cell Rep. *6*, 1139–1152. https://doi.org/10.1016/j.celrep.2014.02.005.

50. Li, Y.I., Sanchez-Pulido, L., Haerty, W., and Ponting, C.P. (2015). RBFOX and PTBP1 proteins regulate the alternative splicing of micro-exons in human brain transcripts. Genome Res. *25*, 1–13. https://doi.org/10.1101/gr.181990.114.

51. Busskamp, V., Lewis, N.E., Guye, P., Ng, A.H., Shipman, S.L., Byrne, S.M., Sanjana, N.E., Murn, J., Li, Y., Li, S., et al. (2014). Rapid neurogenesis through transcriptional activation in human stem cells. Mol. Syst. Biol. *10*, 760. https://doi.org/10.15252/msb.20145508.

52. Arias-Cavieres, A., Khuu, M.A., Nwakudu, C.U., Barnard, J.E., Dalgin, G., and Garcia, A.J., 3rd (2020). A HIF1a-dependent pro-oxidant state disrupts synaptic plasticity and impairs spatial memory in response to intermittent hypoxia. eNeuro *7*. ENEURO.0024-20.2020. https://doi.org/10.1523/ENEURO.0024-20.2020.

Please cite this article in press as: Yang et al., Upregulation of *SYNGAP1* expression in mice and human neurons by redirecting alternative splicing, Neuron (2023), https://doi.org/10.1016/j.neuron.2023.02.021

STAR★METHODS

KEY RESOURCES TABLE

REAGENT or RESOURCE	SOURCE	IDENTIFIER
Antibodies		
Anti-Syngap1 (C terminal)	Thermo Fisher	Cat# PA1-046; RRID: AB_2287112
Anti-Syngap1 (N terminal)	Thermo Fisher	Cat# PA5-37909; RRID: AB_2554517
Anti-mCherry	MyBioSource	Cat# 12158167001; RRID: AB_2827808
Anti-Ptbp1	Abcam	Cat# ab5642; RRID: AB_305011
Anti-Ptbp2	Millipore	Cat# ABE431; RRID: AB_2928034
Anti- GAPDH	Cell Signaling	Cat# 97166S; RRID: AB_2756824
Chemicals, peptides, and recombinant proteins		
Cycloheximide solution	Sigma-Aldrich	Cat# C4859-1ML
Doxycycline hyclate, ≥98% (HPLC)	Sigma-Aldrich	Cat# D9891-1G
NotI-HF	NEB	Cat# R3189L
AscI	NEB	Cat# R0558L
Phusion Hot Start II High-Fidelity DNA Polymerase	Thermo Fisher	Cat# F537S
FuGENE HD Transfection Reagent	Promega	Cat# E2311
Lipofectamin 2000	Thermo Fisher	Cat# 12566014
Novex 4-12% Tris-Glycine Mini Gels	Thermo Fisher	Cat# XP04122BOX
Novex TBE Gels, 8%	Thermo Fisher	Cat# EC6215BOX
Critical commercial assays		
TnT SP6 High-Yield Wheat Germ Protein Expression System	Promega	Cat# L3260
Quick-RNA MiniPrep	Zymo	Cat# R1054
GeneJET Genomic DNA Purification Kit	Thermo Fisher	Cat# K0721
TruSeq RNA Library Prep Kit	Illumina	Cat# RS-122-2001
Alt-R Genome Editing Detection Kit	IDT	Cat# 1075931
SuperScript IV	Thermo Fisher	Cat# 18091050
Gibson Assembly Master Mix	NEB	Cat# E2611S
Quick Ligation Kit	NEB	Cat# M2200S
Deposited data		
Mouse cortical neurons and neural progenitors RNA-seq	This study	BioProject ID: PRJNA930469
Experimental models: Cell lines		
Neuro2a	ATCC	Cat# CCL-131
SYNGAP1-mutant iPSCs (333del, Lys114SerfsX20)	SFARI	Cat# 15209-x1
iNGN	Benoit Laurent lab, Université de Sherbrooke	N/A
NA19101	Marcelo A. Nobrega lab, The University of Chicago	N/A
28126	Yoav Gilad lab, The University of Chicago	N/A
21792	Yoav Gilad lab, The University of Chicago	N/A
Primary mouse neurons	This study (from E18.5 CD1 mouse embryos or neonatal pups)	N/A

(*Continued on next page*)

Please cite this article in press as: Yang et al., Upregulation of *SYNGAP1* expression in mice and human neurons by redirecting alternative splicing, Neuron (2023), https://doi.org/10.1016/j.neuron.2023.02.021

Continued

REAGENT or RESOURCE	SOURCE	IDENTIFIER
Experimental models: Organisms/strains		
Syngap1 conditional knockout mouse	The Jackson Laboratory	Cat# 029303, RRID: IMSR_JAX:029303
Emx1-Cre mouse	The Jackson Laboratory	Cat# 005628, RRID: IMSR_JAX:005628
Syngap1-NISO mouse	This study	N/A
Oligonucleotides		
Nucleotide synthesis	IDT	https://www.idtdna.com/pages
Software and algorithms		
STAR 2.7	PMID: 23104886	https://github.com/alexdobin/STAR
rMATS 3.2.5	PMID: 25480548	http://rnaseq-mats.sourceforge.net/rmats3.2.5/
rMAPS2	PMID: 27174931	http://rmaps.cecsresearch.org/
CLIPSeqTools	PMID: 26577377	https://github.com/mnsmar/clipseqtools
MAFFT v7	PMID: 28968734	https://mafft.cbrc.jp/alignment/server/
Vertebrate RNA-Seq	NIH Genome Data Viewer	RNA-seq tracks for each species

RESOURCE AVAILABILITY

Lead contact

Further information and requests for resources and reagents should be directed to and will be fulfilled by the lead contact, Xiaochang Zhang (xczhang@uchicago.edu).

Materials availability

All unique/stable reagents generated in this study are available from the lead contact with a completed Materials Transfer Agreement.

Data and code availability

- The RNA sequencing results shown in Figure 1A have been uploaded to NCBI (PRJNA930469: SRR23308049, SRR23308050). The microscopy data reported in this paper will be shared by the lead contact upon request.
- This study does not generate new code.
- Any additional information required to reanalyze the data reported in this paper is available from the lead contact upon request.

EXPERIMENTAL MODEL AND SUBJECT DETAILS

Animals

Mouse protocols were reviewed and approved by the University of Chicago Institutional Animal Care and Use Committee. Animals were housed under 12 hours light/dark cycles and supplied with food and water ad libitum.

Guide RNAs (SG321 and SG322) flanking the designed *Syngap1* deletion region were selected with the CRIPSOR online tool. Guide RNAs, tracrRNA, and Cas9 protein were purchased from IDT. Guide RNAs were annealed with tracrRNA, mixed with Cas9 protein in the injection buffer, and injected into C57BL/6 mouse zygotes by the Transgenic Core (University of Chicago). Founder mice were PCR screened for the deletion and positive founders were bred with C57BL/6 (Charles River) to obtain positive F1s, which were further mated with C57BL/6 for positive F2s. F2s and later generations were used in this study. The *Syngap1-NISO* allele is genotyped using primers SG245F-SG331R-SG202R, and the expected product sizes are: wild-type allele is 405bp (and weak 761bp), and the NISO N allele is 493 bp. The *Syngap1* conditional knockout (cKO, Jax#029303) and *Emx1-Cre* (Jax#005628) mice were obtained from the Jackson Lab and genotyped following providers' protocols.

Primary cell culture

Primary hippocampal neurons or cortical neurons were isolated from E18.5 CD1 mouse embryos or neonatal pups with Papain (Worthington). Primary neurons were plated onto poly D-lysine coated coverslips and cultured following standard protocols (Neurobasal medium supplemented with GlutaMax, N2, B27, and 1μM AraC during DIV1-DIV3).

Human iPSCs

iPSC lines, including PGP1-iNGN,[51] 28126, 21792 (Yoav Gilad lab at The University of Chicago), and NA19101 (Marcelo A. Nobrega lab at The University of Chicago), were grown in Essential 8 (Thermo Fisher, A1517001) with penicillin-streptomycin (100U/mL,

Thermo Fisher, 15140122) in 10-cm dishes coated with GelTrex (Thermo Fisher, A1413301) in an incubator at 37 °C with 5% CO_2. Instead of Essential 8, *SYNGAP1*-mutant (Lys114SerfsX20, Simons Foundation) iPSCs were grown in StemFlex (Thermo Fisher, A3349401). Rock inhibitor Y-27632 dihydrochloride (10 μM, Tocris, 1254) was added into culture media for 24 hours after passage. For neuron induction, PGP1-iNGN iPSCs were grown in Essential 8 supplemented with doxycycline (1μg/mL, Sigma-Aldrich, D9891) and penicillin-streptomycin (100 U/mL) for 4 days. To analyze the NMD-transcript of *SYNGAP1*, iPSCs cells and iPSC-derived neurons were treated with cycloheximide (200 μg/mL dissolved in DMSO) for 5 hours in 12-well plates with 1 mL culture media in each well, followed by RNA extraction and analyses.

Cerebral organoids

Induction of brain organoids was performed according to published protocols.[43] Briefly, 3×10^6 human iPSCs (28126 and 21792) were seeded per AggreWell 800 well (STEMCELL Technologies, 34815) in Essential 8 supplemented with Y-27632 dihydrochloride (10 μM) (Tocris, 1254) and penicillin-streptomycin (100 U/mL). 24 hours later, iPSC spheroids were transferred into ultra-low attachment 6-well plates and then incubated in Essential 6 supplemented with dorsomorphin (2.5 μM) (Sigma-Aldrich, P5499) and SB-431542 (10 μM) (Tocris, 1614) for 6 days to induce neural spheroids. Then the neural spheroids were incubated in Neurobasal A medium (Thermo Fisher Scientific, 10888022) supplemented with B-27 without vitamin A (1:50) (Thermo Fisher Scientific, 12587010), GlutaMax (1:100) (Thermo Fisher Scientific, 35050-061), epidermal growth factor (EGF) (20ng/mL) (R&D Systems, 236-EG), basic fibroblast growth factor (bFGF) (20ng/mL) (R&D Systems, 233-FB) and penicillin-streptomycin (100 U/mL) for 19 days, after which the EGF and bFGF were replaced by brain-derived neurotrophic factor (BDNF) (20ng/mL) and NT-3 (20ng/mL) for 18 days. From the 43rd day, brain organoids were incubated in Neurobasal A media supplemented with B-27 without vitamin A (1:50), GlutaMax (1:100) and penicillin-streptomycin (100 U/mL) for long-term culture.

Fetal cortical tissue

De-identified frozen fetal human cortical tissues were obtained from the NIH Neurobiobank at the University of Maryland (Baltimore, MD), microdissected, and subjected to RNA extraction. The works described here involving de-identified postmortem tissues were reviewed and approved by The University of Chicago Institutional Review Board.

METHOD DETAILS

Molecular cloning

To detect the A3SS with RT-PCR, the human *SYNGAP1* alternative exon11 was amplified with primer pairs CH748-CH749, and the mouse *Syngap1* A3SS was amplified with primer pairs CH743-CH744.

pCAG-SYNGAP1 (N-terminus). The N-terminal *SYNGAP1* coding sequence was amplified using SG020 and SG022 and inserted into pCZ01 using Gibson Assembly (NEB). pCZ01 is a modified *pCAG-IG* vector described previously.[22]

pCAG-HA-Flag-PTBP1-IRES-mCherry: *PTBP1* cDNA was amplified with CH448-CH422-2, digested with AscI and NotI, and ligated into linearized *pCAG-HA-Flag-IRES-mCherry*.

For *in vitro* translation, *PTBP1* cDNA was amplified using primer pair SG209-SG210. To knock down Ptbp1/2, shRNA lenti-vectors were used as described previously.[22]

The *SYNGAP1* wild-type mini-gene construct spanning exon9 through exon12: genomic DNA extracted from HEK293FT cells was amplified with primer pairs SG085-SG086 and the purified PCR product was inserted to pCZ01 using Gibson Assembly (NEB).

SYNGAP1 mini-gene deletion constructs: To delete the deep intronic element, two fragments were amplified using PCR primer pairs SG159-SG086 and SG160-SG085, and inserted into linearized pCZ01 using Gibson Assembly.

To delete predicted U2AF65 binding site #1, two fragments were amplified using PCR primer pairs SG155-SG086 and SG156-SG085, and inserted into pCZ01.

To delete predicted U2AF65 binding site #1 + extended, two fragments were amplified using PCR primer pairs SG095-SG086 and SG098-SG085, and inserted into pCZ01.

To delete the A3SS, two fragments were amplified using PCR primer pairs SG087-SG086 and SG088-SG085, and inserted into pCZ01.

To delete predicted U2AF65 binding site #2, two fragments were amplified using PCR primer pairs SG089-SG086 and SG090-SG085, and inserted into pCZ01.

SYNGAP1 mini-gene with patient mutations: To introduce the mutation c.1676 +5 G>A (NM_006772.2), two fragments were amplified using PCR primer pairs SG189-SG086 and SG190-SG085, and inserted into pCZ01.

To introduce the mutation c.1677-2_1685del, two fragments were amplified using PCR primer pairs SG191-SG086 and SG192-SG085, and inserted into pCZ01.

Plasmids were transfected into Neuro2a cells (ATCC) with Lipofectamine 2000 (Thermo Fisher), selected by puromycin and total RNA was extracted with Trizol (Sigma). Reverse transcription was performed with random primers following manufacturer's protocols (Superscript IV, Thermo Fisher). Primers sequences are listed in Table S1.

Please cite this article in press as: Yang et al., Upregulation of *SYNGAP1* expression in mice and human neurons by redirecting alternative splicing, Neuron (2023), https://doi.org/10.1016/j.neuron.2023.02.021

RT-PCR and Western blot

For RNA extraction, brain tissues, or culture cells were dissolved in TRIzol by firmly pipetting and then subjected to either precipitation or Direct-zol RNA Purification Kit. For Western blotting, protein lysates were extracted with RIPA buffer (Thermo Fisher, PI89901) supplemented with proteinase inhibitors (Sigma-Aldrich, 11836170001). Protein samples were loaded onto SDS-PAGE gels, transferred to PVDF membranes, incubated with primary and secondary antibodies successively (Key Resources Table), and then imaged using the LI-COR Odyssey system (LI-COR, 9142).

EMSA

Cy5 conjugated RNA probes (SG-probe1/2) and unlabeled cold competitors of potential PTBP1 binding sites were synthesized by IDT. PTBP1 protein was produced by TnT SP6 High-Yield Wheat Germ Protein Expression System (Promega). *In vitro* translated PTBP1 was diluted in the RNA-protein binding solution, incubated with Cy5 probes with or without cold competitor probes, and resolved on 8% TBE gels (Thermo Fisher, EC6215BOX). The gel was directly visualized with a Typhoon imaging system.

Mouse behavioral tests

Barnes maze test was performed following published protocols.[39,52] Motor coordination and balance of mice (aged around 2 months to 4 months) were examined by Rotarod tests: mice were gently placed on a rotatable rod (Columbus Instruments, ECONOMEX) that was accelerated at 0.2 rpm/second from 5 rpm over a 3-minute period. Time from rotation start to mouse fall in each trial was recorded as the latency to fall. Three trials were performed for each mouse on the test day.

fEPSP recordings

Acute hippocampal slices were prepared from young adult (1-2.5 months) male mice, which were anesthetized with isoflurane and euthanized by rapid decapitation. The brain was rapidly harvested and blocked, rinsed with cold artificial cerebrospinal fluid (aCSF) and mounted for vibratome sectioning. The mounted brain tissue was submerged in aCSF (4°C; equilibrated with 95% O_2, 5% CO_2) and coronal cortico-hippocampal brain slices (350 μm thick) were prepared. Slices were immediately transferred into a holding chamber containing aCSF equilibrated with 95% O_2, 5% CO_2 (at 20.5±1°C). Slices were allowed to recover a minimum of one hour prior to the transfer into recording chamber and were used within eight hours following tissue harvest. The composition of aCSF (in mM):118 NaCl, 10 Glucose, 20 sucrose, 25 $NaHCO_3$, 3.0 KCl, 1.5 $CaCl_2$, 1.0 NaH_2PO_4 and 1.0 $MgCl_2$. The osmolarity of aCSF was 305-315 mOsm and equilibrated, and the pH was 7.42±0.02.

The extracellular recording of the fEPSP was established in aCSF (31.0 ± 2°C, equilibrated with 95% O_2 5% CO_2) superfused and recirculated over the preparation. The stimulation electrode, a custom constructed bipolar electrode composed of twisted Teflon coated platinum wires (wire diameter: 127 μm, catalog number 778000, AM Systems.), was positioned in the Schaffer Collateral and the recording electrode (1-2 MΩ) was placed into the stratum radiatum of the CA1. The intensity of the electrical current (100-400 μA; 0.1-0.2 ms duration) was set to the minimum intensity required to generate the 50% maximal fEPSP. After 10 minutes of recording the baseline fEPSP, LTP was induced using Theta Burst Stimulation (TBS: four trains of 10 bursts at 5 Hz, each burst was comprised four pulses at 100 Hz). Following stimulation, recordings continued for up to one hour. The fEPSP slope was normalized to baseline values. Recordings were made using either a Multiclamp 700B (Molecular Devices) or using a differential amplifier (AM system).

Whole-cell patch-clamp recordings

Slices from primary somatosensory cortex (S1; 350μm thick) were prepared from young mice (postnatal day 16-28) after isoflurane anesthesia and decapitation. The procedure was described in detail before[46] and is in accordance with the guidelines of the Animal Care and Use Committee of the University of Chicago. The slices were cut on a vibratome (Leica VT1000S) using ceramic blades. To preserve thalamocortical projections, slices were cut at a 55° angle to the right (posterior) of the anterior-to-posterior axis of the brain (see Agmon and Connors, 1991). The slices were cut in a sucrose slicing solution containing the following (in mM): 185 sucrose, 2.5 KCl, 25 glucose, 25 $NaHCO_3$, 1.2 NaH_2PO_4, 0.5 $CaCl_2$, and 0.5 $MgCl_2$, bubbled with 95% O_2 and 5% CO_2. Following slicing, the slices were kept in artificial cerebrospinal fluid (ACSF) containing the following (in mM): 124 NaCl, 5 KCl, 1.25 NaH_2PO_4, 2 $CaCl_2$, 2 $MgSO_4$, 26 $NaHCO_3$, and 10 D-glucose, bubbled with 95% O_2 and 5% CO_2. The slices were allowed to recover for at least 1h and were subsequently transferred to a submerged recording chamber superfused with ACSF at elevated temperature (28-30°C). Whole-cell patch-clamp recordings were performed under visual control using a 40x water-immersion objective in combination with near-infrared light illumination (IR-DIC) and a Zeiss AxioCam MRm camera mounted on a Zeiss Examiner A1 microscope (Carl Zeiss MicroImaging). Patch pipettes (~2.5-4.5 MΩ) were filled with internal saline containing the following (in mM): 9 KCl, 10 KOH, 120 K-gluconate, 3.48 $MgCl_2$, 10 HEPES, 4 NaCl, 4 Na_2ATP, 0.4 Na_3GTP, and 17.5 sucrose, pH adjusted to 7.25. Patch-clamp recordings were performed in current-clamp mode using an EPC-10 amplifier (HEKA Electronics). Input resistance (Ri) was measured by injection of hyperpolarizing test currents (100pA, 100ms). For all recordings and analyses, we used a blind approach, in which the researcher was ignorant of the mouse genotype. Data obtained from the patch-clamp recordings were analyzed using Pulsefit (HEKA Electronics), Igor Pro (WaveMetrics) and MatLab. For statistical comparison of action potential-related parameters between genotypes, we used the one-way ANOVA. A two-way ANOVA test was used to examine statistical relationships between a) genotypes and b) genotypes x current amplitude in the input (current injection) - output (spike number) measurements.

Please cite this article in press as: Yang et al., Upregulation of *SYNGAP1* expression in mice and human neurons by redirecting alternative splicing, Neuron (2023), https://doi.org/10.1016/j.neuron.2023.02.021

Primary neuron transfection and immunostaining

Primary neurons were transfected by Lipofectamine 2000 (Thermo Fisher) or jetOPTIMUS (Polyplus). For immunostaining, primary neurons were fixed for 10 minutes in 4% paraformaldehyde (PFA) at 4°C, rinsed with 1x PBS, and incubated with blocking buffer (1x PBS containing 0.03% Triton X-100 and 5% normal donkey serum) in room temperature for 30 mins, and further incubated with primary antibodies diluted in PBST buffer (1x PBS containing 0.03% Triton X-100) overnight at 4°C. After 3 times washing with 1x PBS, slides were incubated for one hour at room temperature with fluorophore-conjugated secondary antibodies in the dark. Slides were scanned with a Leica SP8 confocal microscope. The antibodies were listed in the Key Resources Table.

Splice-switching oligonucleotides

SSOs were synthesized by Integrated DNA Technologies (IDT). For SSO transfection, 4×10^5 cells were seeded in 12-well plates coated with GelTrex (Thermo Fisher, Gibco, A1413301). 200nM SSOs were transfected into cells using TransIT-LT1 Transfection Reagent (Mirus, MIR2300) according to the manufacturer's instructions. Brain organoids derived from iPSC 28126 were treated by three doses of SSOs (300nM) from day 133 to 137. On day 139, RNA and protein were extracted from brain organoids for PCR and western blot analyses. For brain organoids derived from iPSC 21792, they were treated by five doses of SSOs (200nM) from day 169 to 173. RNA and protein were extracted on day 174. Total RNA was extracted using TRIzol reagent (Thermo Fisher, 15596018) and Direct-zol RNA Purification Kit (Zymo Research, R2060) 24 hours after transfection. cDNA was synthesized by SuperScript IV Reverse Transcriptase kit (Thermo Fisher, 18090050). Quantitative PCR (Q-PCR) was performed using SYBR Green PCR Master Mix (Thermo Fisher, 4344463) in QuanStudio Real-Time PCR Systems (Thermo Fisher, ZG11CQS3STD) according to manufacturers' instructions.

QUANTIFICATION AND STATISTICAL ANALYSIS

To identify differential splicing events, we analyzed at least two biological replicates for each genotype using rMATS and filtered by False Discovery Rate (FDR)<0.05 and |differential PSI|>10%. CLIP-Seq data were aligned and mapped to the mouse (mm10) or human (hg38) genomes by CLIPSeqTools, using the default parameters. The aligned files were visualized in IGV. CLIP-Seq datasets used in this study: PTBP1_ESC (SRR2121761), PTBP1_NPC (SRR2121762), U2AF65 (ERR208893, ERR208897, GSE83923), PTBP2 (SRR871026, SRR871030). Multiple Sequence Alignment Genome sequences of multiple vertebrates were obtained from NCBI HomoloGene database. Multiple sequence alignment and phylogeny analysis were performed by MAFFT over the conserved region of *SYNGAP1* intron10. The splice site usage was validated by RNA-Seq data of non-neuronal tissues from the corresponding species. Comparisons of electrophysiology recordings were assessed by a one-way ANOVA followed by the Bonferroni correction in Prism (GraphPad). Comparisons of mouse behaviors and Q-PCR results were done with Tukey's multiple comparisons in Prism, and the adjusted p-values were indicated.